PNNL-23764

Loads as a Resource

Frequency Responsive Demand

September 2014

K Kalsi
J Lian
LD Marinovici
M Elizondo
W Zhang
C Moya

U.S. DEPARTMENT OF ENERGY

Prepared for the U.S. Department of Energy
under Contract DE-AC05-76RL01830

DISCLAIMER

PACIFIC NORTHWEST NATIONAL LABORATORY
operated by
BATTELLE
for the
UNITED STATES DEPARTMENT OF ENERGY
under Contract DE-AC05-76RL01830

Printed in the United States of America

Available to DOE and DOE contractors from the
Office of Scientific and Technical Information,
P.O. Box 62, Oak Ridge, TN 37831-0062;
ph: (865) 576-8401
fax: (865) 576-5728
email: reports@adonis.osti.gov

Available to the public from the National Technical Information Service
5301 Shawnee Rd., Alexandria, VA 22312
ph: (800) 553-NTIS (6847)
email: orders@ntis.gov <http://www.ntis.gov/about/form.aspx>
Online ordering: http://www.ntis.gov


This document was printed on recycled paper.
(8/2010)

PNNL-23764

Frequency Responsive Demand

K Kalsi
J Lian
LD Marinovici
M Elizondo
W Zhang
C Moya

September 2014

Prepared for
the U.S. Department of Energy
under Contract DE-AC05-76RL01830

Pacific Northwest National Laboratory
Richland, Washington 99352

Executive Summary

Frequency control plays an important role in preserving the power balance of a multi-machine power system. Generators modify their power output when a non-zero frequency deviation is presented in order to restore power balance across the network. However, with plans for large-scale penetration of renewable energy resources, performing primary frequency control using only supply-side resources becomes not only prohibitively expensive, but also technically difficult. Frequency control from the demand side or load control presents a novel and viable way for providing the desired frequency response. Loads can measure frequency locally and change their power consumption after a non-zero frequency deviation is presented in order to achieve power balance between generation and consumption. The specific objectives of this project are to:

- Provide a framework to facilitate large-scale deployment of frequency responsive end-use devices
- Systematically design decentralized frequency-based load control strategies for enhanced stability performance
- Ensure applicability over wide range of operating conditions while accounting for unpredictable end-use behavior and physical device constraints
- Test and validate control strategy using large-scale simulations and field demonstrations
- Create a level-playing field for smart grid assets with conventional generators

Next, a brief recap of FY12 and FY13 activities is presented followed by the progress made on the FY14 tasks.

In FY12, a study [1] was performed to demonstrate that autonomous demand response can provide substantial benefit by responding to under-frequency events in the interconnected power system. In addition, the study demonstrated that the characteristics of frequency response delivered by autonomous demand response are analogous to generator governor action. The study assumed a fixed proportional response between power and frequency, which may not always be the best control strategy to ensure stability over varying system conditions. Furthermore, there was no systematic way of designing gains to ensure stability over wide range of operating conditions. Finally, the study assumed simplistic models for the end-use loads, ignoring end-use behavior and physical device constraints.

In FY 13, a systematic approach was proposed in [2] for a demand-side primary frequency strategy to regulate the frequency of the system to its nominal value and restore power balance for a multi-machine power system model. The load control law was designed in a hierarchically decentralized manner consisting of two interactive decision layers. In the first layer, a supervisory controller is responsible to gather system level information (e.g., power flow, system topology, generation and load forecast, available responsive loads, among others), and determine the optimal gains for the responsive loads on each bus every few (e.g., 15-30) minutes. In the second layer, each decentralized load switched ON/OFF probabilistically in real time based on local frequency measurement so that the aggregated load response under each bus matches the desired power determined by the first layer. The control gain design in the

first layer was based on the decentralized robust control theory, while the load switching probabilities were designed using Markov chains. The proposed decentralized robust control strategy was tested as a proof-of-concept using IEEE test systems in the MATLAB Power Systems Toolbox (PST). Autonomous responses are critical for many reliability purposes where there may not be time to communicate needed actions through wide-area network.

In FY14, the controller design proposed in FY13 was extended to deal with more realistic power system models. The design framework proposed in FY13 assumed that load control strategies are based on local angle and frequency measurement. In reality, the angle cannot be directly measured, and does not provide much useful information about the system behavior. In FY14, the local response rules were modified so that the controller only uses information on frequency deviation and its derivatives. The existing design of demand-side droop gains is based on network-reduction power system models, for which load buses are suppressed and combined with nearby generator buses. In FY14, the framework was extended to include network-preserving power system models. This will allow the design to fully respect the topology of the power system network, which is crucial for primary frequency control problems. Such an extension is highly nontrivial as the load bus transient frequency dynamics and their interactions with the generation side dynamics have not been well studied in the literature. Another major task in FY14 was to implement the modified control strategies on the Western Electricity Coordinating Council (WECC) model using PowerWorld. Simulation studies and performance metrics were designed to analyze the impacts of large-scale deployment of frequency responsive load.

A rigorous theoretical analysis was performed to prove the closed-loop system stability under demand-side frequency control. Specifically, it was shown that with only local frequency measurement, the frequency synchronization and asymptotic stability around post-fault equilibrium can still be satisfied as long as the control gains were chosen to be non-negative. The extended hierarchical demand-side frequency control was tested in four simulation cases in the WECC system: i) comparison with and without load control, ii) sensitivities to control gain parameters, iii) location of controllable load, and iv) type of end-use devices being controlled. The results indicated that the proposed frequency-based load control strategy showed improved frequency recovery in terms of steady state error and maximum frequency deviation. The simulations showed that the response of intertie power flows depended on relative location of disturbance and responsive load and generation. An important aspect of the enhanced frequency-based load control strategy was that the control gain can be adapted, by the system operator from the supervisory control level, based on the available controllable load resources and changing operating conditions.

Another objective in FY13, as detailed in [2], was to perform extensive simulation studies to investigate the impact of a population of autonomous Grid Friendly™ Appliances (GFAs) on the bulk power system frequency stability. A preliminary investigation of the grid impacts of the GFA design indicated that the location of GFAs affected system stability performance. Also, the impact of location was coupled with effects of the GFA time delay parameter. In FY14, a major goal in terms of modeling and controls of GFAs was to improve the GFA control design such that the aggregate response mimicked a generator droop like response. It was shown that when the actual distribution of the pre-determined thresholds is biased, it could potentially impact the system response negatively. One possible solution was to introduce a supervisor at each distribution feeder to modify the thresholds of the GFAs in a way so as to follow a proportional response.

Acknowledgments

The authors are grateful for the comments and feedback provided by Jason Fuller, Jeff Dagle and Frank Tuffner at the Pacific Northwest National Laboratory.

Acronyms and Abbreviations

GFAs	Grid Friendly™ Appliances
TCL	Thermostatically Controlled Loads
HVAC	Heating, Ventilation, and Air Conditioning
PST	Power System Toolbox
PNNL	Pacific Northwest National Laboratory
LMI	Linear Matrix Inequality
WECC	Western Electricity Coordinating Council

Table of Contents

Figures

1.0 Introduction

In the conventional power grid paradigm, system generation is actively controlled to match the system load that is passive most of the time. End-use loads are generally not controlled unless the system is experiencing severe stability issues, which may cause under-frequency load shedding. The transient stability of the power grid is primarily maintained by droop control of synchronous generators through speed governors. However, the conventional load-following control strategy becomes less effective in maintaining the system stability under high penetration of intermittent renewable energy such as wind energy and solar energy. This is because of reduced system inertia and damping with the increasing penetration of renewable generation that has very small, or no, rotating mass. Demand-side frequency control presents a novel and viable way for providing the desired frequency response. Loads can measure frequency locally and change their power consumption after a non-zero frequency deviation is observed, in order to achieve power balance between supply and demand. Several load control implementations have been proposed [3]-[7]. In all the aforementioned approaches, frequency control was based on overly-simplified power system models (such as lumped linear system model or multi-machine model with DC power flow). In addition, device constraints and end-use behavior (such as compressor time delays for thermostically controlled loads, and stochastic load arrival and departure) have not been considered in a systematic manner in the controller design. These constraints can significantly influence the aggregated response of the controllable devices, and thus impact the overall frequency dynamics. Furthermore, most previous approaches cannot deal with time-varying system conditions, such as power flow across the network, available responsive loads, changing network topology, and renewable generations, among others.

In FY13, a hierarchical robust demand-side frequency control framework was proposed that systematically accounted for the interactions between the total load response and the bulk power system frequency dynamics. At the supervisory control layer, the optimal feedback gains required from the aggregated load response on each bus are computed by solving Linear Matrix Inequalities (LMIs). The decentralized-robust controller-based design ensures the stability of the closed-loop system over a wide-range of operating conditions. The systematic computation of the gains every few minutes in the supervisory control layer allows for an adaption to time-varying system operating conditions. At the device layer, the mode switching probabilities of individual devices are computed based on the Markov-chain model and the measured frequency deviation so that the total population response matches the desired one determined by the supervisory controller. The Markov-chain-based design of local load response rules can fully respect the device constraints (such as temperature setpoint, compressor time delays of Heating, Ventilation, and Air Conditioning (HVAC) units, arrival and departure of the deferrable loads, etc.), which are crucial for implementing real load control programs. The proposed hierarchical, decentralized frequency control strategy was implemented and tested on the IEEE 16-machine, 86-transmission line, 68-bus power system using the Power System Toolbox (PST) in MATLAB. The results indicated that the proposed demand-side frequency control strategy can greatly improve the system damping, restore the system frequency under contingencies and achieve a desired steady-state system response while taking into account the physical constraints of end-use loads at the same time.

There were three main problems associated with the overall frequency-based load control framework proposed in FY13. First, the controller design was based on a reduced multi-machine power system model, which does not represent the accurate system dynamics. Second, the controller design requires not

only the local frequency, but also the local angle, which makes it impractical. Third, the effectiveness of the proposed load control is guaranteed if the population of end-use loads is sufficiently large. In other words, the proposed load control design does not explicitly consider the limited capabilities of end-use loads. Thus, in FY14, the focus of the work is to modify the design to overcome these issues. In particular, the control design is modified to be based on the structure preserving power system model, instead of the simplified power system model. The resulting load controller also only requires the local frequency measurement which can be easily measured. Furthermore, in order to respect the time-varying capabilities of end-use loads, the control gains are carefully designed by accounting for varying system operating conditions. The modified controller design is implemented on the Western Electricity Coordinating Council (WECC) model using the PowerWorld simulation software. Extensive simulation studies using different scenarios are performed to validate the effectiveness of the newly proposed control design.

The promise of autonomous, Grid Friendly response by smart appliances in the form of under-frequency load shedding was demonstrated in the GridWise Olympic Peninsula Demonstration in [8] and [9]. Grid Friendly™ Appliance (GFA) controllers in the GridWise Olympic Peninsula provided autonomous under-frequency load shedding in dryers and water heaters. Each controller monitored the power grid frequency signal and requested that electrical load be shed by its appliance whenever electric power grid frequency fell below a unique and randomly chosen threshold between 59.95 Hz and 59.985 Hz. The controllers and their appliances responded reliably to each shallow under-frequency event, which was an average of one event per day and shed their loads for the durations of these events. The report presented in [10] studied the dynamic effects of populations of Grid Friendly™ water heater controllers on the power grid during under-voltage and under-frequency events. In particular, models for water heater with GFA controllers were developed using a scripting programming language and simulated in GE Positive Sequence Load Flow (PSLF), a software suite designed to study power systems in both steady-state and dynamic environments. Due to some software limitations, the project wasn't able to simulate any effect that the frequency dependent load could have on the bulk power system. In FY13, extensive simulation studies were performed to study the impact of a population of GFAs on the bulk power system frequency stability. The main conclusions of the study were that:

- Location of GFAs affects system stability performance
- Impact of location is coupled with time delay
- Need further investigation into how many GFAs to deploy across the system

The focus of FY14 was to propose a systematic GFA control design such that aggregate response mimics generator "droop-like" response.

2.0 Extended hierarchical demand-side frequency control strategy

In this section, the hierarchical, frequency-based load control framework proposed in FY13 will be extended by: a) considering network-preserving power system models which will allow the design to fully respect the topology of the power network, b) controller design is only dependent on local frequency and not phase angle, and c) avoid prematurely exhausting the capabilities of end-use loads in response to system frequency deviation. The overall structure of the control strategy remains the same. At the supervisory level, optimal load control gains are derived for each load bus to specify the power modulation command for controllable loads at that bus in order to stabilize the power system during contingencies. At the device level at each load bus, decentralized controllers are designed for each individual device based on Markov Chains so that the change of power consumption of controllable loads matches the desired power modulation command determined at the aggregate level.

2.1 Network-preserving multi-machine power system model

The design of the proposed hierarchical distributed load control strategy requires a multi-machine power system model for the stability analysis. Let θ_i be the voltage phase angle at the i-th bus. Then the active power flow at each bus i, denoted as $f_i(\theta)$ is determined by

$$f_i(\theta) = \sum_{j=1}^{n} b_{ij} \sin(\theta_i - \theta_j) \tag{1}$$

where $b_{ij} = |V_i||V_j|B_{ij}|$ is the maximum power transferred from generator bus i to generator bus j with $|V_i|$ and $|V_j|$ are the regulated voltages at bus i and j, and $|B_{ij}|$ is the admittance of the transmission line between bus *i* and bus *j*. The dynamics of internal generator bus, as detailed in [12], are given by the following differential equation,

$$M_i\ddot{\theta}_i + D_{Gi}\dot{\theta}_i + f_i(\theta) = P^0_{m,i} \tag{2}$$

where M_i is the inertia of the i-th generator, D_{Gi} is the mechanical damping of the i-th generator, and $P^0_{m,i}$ is the nominal mechanical power output of the i-th generator. The load buses are assumed to be frequency-sensitive, hence each load bus has the following dynamics,

$$D_{li}\dot{\theta}_i = -(P_{l,i} + f_i(\theta)) \tag{3}$$

where D_{li} is the damping constant as defined in [13] and [14], and $P_{l,i}$ is the total power consumption of the loads under bus i. At each load bus, it is assumed that there are controllable and uncontrollable loads, with the controllable loads being thermostatically controlled loads (TCLs). Denote the total power consumption of uncontrollable loads as $P_{\text{no-cont},i}$, and the total power consumption of controllable loads as $P_{\text{cont},i}$. The total power consumption of controllable loads can be represented by $P_{\text{cont},i} = P^0_{\text{cont},i} + u_i$, where $P^0_{\text{cont},i}$ is the nominal power consumption of the controllable loads without load control and u_i is the power

modulation when the load control is active. So $P_{l,i}$, which is the total power consumption of all the loads at bus i, can then be given as,

$$P_{l,i} = P_{\text{cont},i} + P_{\text{no-cont},i} = \underbrace{P^0_{\text{cont},i} + P_{\text{no-cont},i}}_{P^0_{l,i}} + u_i \tag{4}$$

where $P^0_{l,i}$ denotes the nominal load power at each bus. Substituting (4) in (3), the dynamics of the load bus i can be described as

$$D_{li}\dot{\theta}_i + u_i + f_i(\theta) = -P^0_{l,i} \tag{5}$$

In summary, using (2) and (5), the overall power system dynamics can be described by the following structure preserving model,

$$M_i\ddot{\theta}_i + D_i\dot{\theta}_i + u_i + f_i(\theta) = P^0_{m,i} - P^0_{l,i} \tag{6}$$

where

$$\begin{cases} M_i > 0,\ D_i = D_{g,i},\ P^0_{m,i} > 0 & \text{if } i = \text{generator bus} \\ D_i = D_{l,i},\ P^0_{l,i} > 0 & \text{if } i = \text{load bus} \\ M = D_i = P^0_{m,i} = P^0_{l,i} = 0 & \text{otherwise} \end{cases}$$

and

$$u_i = \begin{cases} P_{\text{cont},i} - P^0_{\text{cont},i} & \text{if } i = \text{controllable load bus} \\ 0 & \text{otherwise} \end{cases} \tag{7}$$

It is clear that the network topology has been preserved by the above model, which can more accurately represent the transient dynamics of the power system than the multimachine power system model considered in FY13 detailed in [2] and [15].

2.2 Supervisory-level control design

At the supervisory layer, in the goal is to design u_i during each control period I. The power modulation u_i is designed as a feedback control input characterized by a control gain k_i. As opposed to the design proposed in FY13 ([2] and [15]), it is now assumed that the frequency at each load bus i is the only available state. Therefore, the feedback power modulation can be defined as follows,

$$u_i = k_i(w_i - w_0) \tag{8}$$

where w_i is the frequency at the i-th load bus and w_0 is the nominal frequency of the overall system. In [2] and [15], it was shown that if the power modulation is based on frequency and angle measurements, then demand-side frequency control can achieve robust stability with respect to the pre-fault equilibrium conditions, and the corresponding control gains can be computed using LMIs. Formulating and solving the LMIs requires considerable global information about the power system. With only local frequency measurement, the frequency synchronization and asymptotic stability around post-fault equilibrium can still be satisfied under very mild conditions as will be discuss next.

2.2.1 Stability analysis

Before presenting the proposed demand-side frequency control strategy, this subsection develops and discusses some important stability properties for the network-preserving power system model under demand-side frequency control. These theoretical arguments and results will provide fundamental insights into the closed-loop stability behavior under demand-side frequency control. In particular, it will be shown that if the post fault equilibrium of the power system without demand-side frequency control is asymptotically stable, then the post-fault equilibrium of the power system coupled with demand-side frequency control is also asymptotically stable, if the gains k_i are selected to be nonnegative. For traditional stability analysis, one of the generator buses is typically assumed to be an infinite bus whose frequency does not change much. However, the synchronized frequency after a disturbance may differ from the original frequency of any bus in the system.

For the power system model given in (6), it can be easily verified using (8) that,

$$\sum_{i=1}^{n} M_i \dot{w}_i + \sum_{i=1}^{n} (D_i + k_i) w_i = \sum_{i=1}^{n} P_i + k_i w_0 \tag{9}$$

where $P_i = P_{m,i} - P_{l,i}$ for $i = 1,\ldots,n$. Upon synchronization, $\dot{w}_i = 0$ for all i. Hence, the only possible synchronized frequency w_{sync} is given by

$$w_{sync} = \frac{\sum_{i=1}^{n} (P_i + k_i w_0)}{\sum_{i=1}^{n} (D_i + k_i)} \tag{10}$$

It can be seen that the synchronized frequency depends on the net power injection P_i, the overall damping constant $D_i + k_i$, and the reference frequency w_0. Modifying the control gain k_i will certainly change the synchronized frequency until AGC restores the frequency by modifying the net power injections. To study system frequency stability, it is often convenient to work with relative coordinates. Define the following change of coordinates $w_i^r = w_i - w_{sync}$ and $\theta_i^r = \theta_i - w_{sync} t$. Under the new coordinates, the system defined in (6) can be written as follows,

$$\begin{cases} (D_i + k_i)\dot{\theta}_i^r = q_i(k) - f_i(\theta^r), & i\text{=load bus} \\ \dot{\theta}_i^r = w_i^r, \;\; M_i \dot{w}_i^r + (D_i + k_i) w_i^r = G_i(k) - f_i(\theta^r), & i\text{=generator bus} \end{cases} \tag{11}$$

where $q_i(k) = P_i - (D_i + k_i) w_{sync} + k_i w_0$ is a function of the overall gain vector $k = [k_1,\ldots,k_n]^T$. Note that w_{sync} is also a function of the entire gain vector. Once the gain vector k is chosen and fixed, $q_i(k)$ and w_{sync} become known constants. It can be verified directly from the definitions of $q_i(k)$ and w_{sync} that $\sum_{i=1}^{n} q_i(k) = 0$ for all possible k. Without loss of generality, it can be assumed that buses $1,\ldots,n_g$ are generator buses. The system states given in (11) consist of the angles of all the buses and the frequency of generator buses, i.e., $x = (\theta^r, w^{rg})$, where $w^{rg} \triangleq \left[w_1^r,\ldots,w_{n_g}^r \right]^T$ denotes the frequency vector of generator buses. It can be easily seen from (11) that if is an equilibrium state, it must satisfy

$$q_i(k) = f_i(\theta^r), \forall i \;\text{ and } w_i^{rg} = 0 \text{ for } i = 1,\ldots,n_g \tag{12}$$

Clearly, the control gain k affects both the location of the equilibrium point, as well as the stability property of the corresponding equilibrium. It is important to study the impact of the load control gain on system stability properties. To this end, define

$$\begin{aligned} &f(\theta^r) = [f_1(\theta^r),\ldots, f_n(\theta^r)]^T, D(k) = diag\{D_1 + k_1,\ldots, D_n + k_n\} \\ &q(k) = \left[q_1(k),\ldots,q_n(k)\right]^T \end{aligned} \tag{13}$$

where, $D(k)$ is a diagonal matrix depending on the control gains. Let $(\theta^r(k), 0)$ be the post-fault equilibrium corresponding to control gain k. Namely, $\theta^r(k)$ is the solution to the power flow equation $q(k) = f\left(\theta^r(k)\right)$. It has been shown in [16] that $(\theta^r(k), 0)$ is locally asymptotically stable **if and only if** $\theta^r(k)$ is a locally asymptotically stable equilibrium of the corresponding first-order system given by

$$(D_i + k_i)\theta_i^r = q_i(k) - f_i(\theta^r), \forall i = 1,\ldots,n \tag{14}$$

Re-writing (14) in vector form yields,

$$D(k)\cdot\theta^r = q(k) - f\left(\theta^r\right) \Rightarrow \theta^r = -D(k)^{-1} f\left(\theta^r\right) + D(k)^{-1} q(k) \tag{15}$$

It can be easily seen that the **local** stability of the above nonlinear system depends on the eigenvalues of the following Jacobian matrix,

$$J\left(\theta^r\right) = \left[\frac{\partial f_i}{\partial \theta_j^r}\right]_{i\le n,\, j\le n} = \begin{cases} \sum_{k=1}^{n} b_{ik}\cos\left(\theta_i^r - \theta_k^r\right), & \text{if } j = i \\ -b_{ij}\cos\left(\theta_i^r - \theta_j^r\right), & \text{otherwise} \end{cases} \tag{16}$$

With this notation, the local stability of equilibrium $\theta^r(k)$ for system (14) is determined by the eigenvalues of the following linearized system matrix $A(k) \triangleq -D(k)^{-1} J\left(\theta^r(k)\right)$. In other words, the stability impacts of the control gain k essentially depends on how the eigenvalues of $A(k)$ change with the gain vector k. To study such a relation, some important properties of the Jacobian matrix $J(\theta^r)$, which has been studied extensively in the literature as given in [16], will be reviewed next. Specifically, i) $J(\theta^r)$ is positive semidefinite on $\Delta\left(\frac{\pi}{2}\right)$ and ii) $Null\left(J\left(\theta^r\right)\right) = span\{1_n\}$ where 1_n denotes the vector in R^n with all elements equal to 1 and

$$\Delta\left(\frac{\pi}{2}\right) = \left\{\theta^r \in R^n : \left|\theta_i^r - \theta_j^r\right| \le \frac{\pi}{2},\ \forall i, j \text{ there exists a line connecting bus } i, j\right\} \tag{17}$$

It can be easily seen that $f(\theta^r + \alpha 1_n) = f(\theta^r)$, for all $\alpha \in R$. More precisely speaking, by saying the equilibrium point $\theta^r(k)$ is locally exponentially stable, what is actually meant is the corresponding one-dimensional manifold $\{\theta^r(k) + \alpha 1_n : \alpha \in R\}$ is locally exponentially stable. Therefore, it can easily verified that the stability of $\theta^r(k)$, namely, the manifold $\{\theta^r(k) + \alpha 1_n : \alpha \in R\}$, is guaranteed as long as all the non-zero eigenvalues of $A(k)$ are strictly negative. Based on the above properties of $J(\theta^r)$, this requires $D(k)^{-1}$ to be positive definite. A sufficient condition to make the diagonal matrix $D(k)^{-1}$ positive definite is to choose $k_i \ge 0$ for all i. This justifies the claim mentioned at the beginning of this sub-section. It should be noted that the conclusion requires that the gain vector k is chosen such that $\theta^r(k)$ stays inside $\Delta\left(\frac{\pi}{2}\right)$. Namely, the angle difference of any two neighboring buses is less than $\frac{\pi}{2}$.

2.2.2 Design of feedback control gain

Based on the theoretical arguments presented in Section 2.2.1, the control gain can be designed using engineering judgments and heuristics. One approach used to arrive to such heuristic criteria in this report is based on existing criteria to design existing under-frequency load shedding schemes and parameters of the controllable loads. Other ways of selecting the value of the gain should be considered in future work.

The gain (k_i) at a particular bus/substation can be designed to be a function of system quantities (K_{sys}) and quantities corresponding to the controllable load at a local bus (K_b) and given by the following equation,

$$k_i = K_{sys} * K_b = \frac{pct_{max,load} P_{load,sys}}{\Delta f_{min}} * \frac{pct_{cont,ON,i} P_{cont,i}}{P_{cont,sys}} \quad (18)$$

where the system parameters for K_{sys} are:

- $\Delta f_{\min}$ that can be taken as the frequency deviation threshold that activates load control before emergency under-frequency load shedding acts (this threshold is 0.7 or 0.5 Hz in the WECC system as given in [24])
- $pct_{max,load}$ which is the maximum percentage of total system load that should act at $\Delta f_{\min}$. This percentage value can be taken as the value tripped by the first step of emergency under-frequency load shedding (5.6% is used in the WECC system)
- $P_{load,sys}$ is the total system load i.e. including both controllable and non-controllable loads

The parameters for controllable load at a local bus are given to be:

- $P_{cont,sys}$ which is the total controllable load available system-wide
- $P_{cont,i}$ which is the total controllable load available at a substation bus *i*
- $pct_{cont,ON,i}$ which is the percentage of controllable load in ON state at substation bus *i*

The above design of k_i allows the system operator to account for changing operating points (such as total system load, available controllable load at substation bus and system, and percentage of controllable load in ON state). Specifically, the two parameters $\Delta f_{\min}$ and $pct_{cont,ON,i}$ can be tuned to achieve a desired performance. It is important to note that the values of k_i should only be updated when significant changes in the system operating conditions occur. Therefore, updates every tens of minutes would be sufficient to maintain desired performance. The obtained gains k_i are then broadcasted along with the current system operating conditions, to the population of available controllable loads. In the following section, a systematic way to design load frequency response rules is developed. The strategy probabilistically turns ON and OFF each controllable load to match the desired aggregated response determined by u_i.

2.3 Device-level control design

When the system is subject to a contingency, a non-zero frequency deviation occurs at every bus in the system, i.e., $w_i \neq w_0$. The goal of the device layer controller is to design frequency response rules for individual controllable loads so that the aggregated power change matches the desired amount given by u_i. For simplicity, it is assumed that the set of controllable loads is composed only by thermostatically controlled loads (TCLs). Some examples of TCLs are refrigerators, HVACs, water heaters, etc. Due to the inherent thermal energy storage, these loads can be switched ON/OFF for 30 seconds to 1 minute with minimally affecting the end-use performance. The power consumption of the TCLs is assumed to be zero in the OFF state, and is a non-zero constant when in the ON state. The total controllable power consumption at a bus is the sum of the powers of all the controllable TCLs in the ON state on this bus. Therefore, the objective for each controllable load is to calculate its own probability of turning ON or OFF, such that, the change of power consumption of controllable loads by turning ON or OFF at a given bus is equal to the load power modulation command determined at the aggregate level.

2.3.1 Generic Markov-chain model for TCLs

The controllable loads are expected to make independent decisions to change their current operating states in such a way that the actual aggregate load response can match the desired power modulation. To address this problem, a Markov-Chain model is adopted to capture the aggregate load response of controllable loads under control. Consider the population of *N* controllable loads with the maximum capacity denoted by P_i, $i = 1,2,\ldots N$. It is assumed that each controllable load has n operating states with the corresponding capacity denoted by P_i^j with $j = 1,2,\ldots n$. Also, it is assumed that $P_i^j = c_j P_i$ with $0 \le c_j \le 1$ for the same type of controllable loads. For example, $c_j = 1$ implies that the load is currently ON with maximum capacity, and $c_j = 0$ implies that the load is currently OFF. Let $p_j(t_k)$ denote the percentage of the controllable loads that are in the *j*-th operating state at time t_k. Define

$$\boldsymbol{p}(t_k) = \begin{bmatrix} p_1(t_k) & p_2(t_k) & \cdots & p_n(t_k) \end{bmatrix}^{\mathrm{T}} \tag{19}$$

The evolution of the percentages $p_j(t_k)$, can be captured by the following Markov-Chain model,

$$\boldsymbol{p}(t_{k+1}) = \boldsymbol{A}(t_k)\boldsymbol{p}(t_k) \tag{20}$$

where

$$\boldsymbol{A}(t_k) = \begin{bmatrix} 1-\sum_{j\neq 1}\mu_{1j}(t_k) & \mu_{21}(t_k) & \cdots & \mu_{n1}(t_k) \\ \mu_{12}(t_k) & 1-\sum_{j\neq 2}\mu_{2j}(t_k) & \cdots & \mu_{n2}(t_k) \\ \vdots & \vdots & \ddots & \vdots \\ \mu_{1n}(t_k) & \mu_{2n}(t_k) & \cdots & 1-\sum_{j\neq n}\mu_{nj}(t_k) \end{bmatrix} \tag{21}$$

and $\mu_{ij}(t_k)$ denotes forced switching probability from the i-th operating state to the j-th operating state at t_k. The aggregate load power $P(t_k)$ is given by

$$P(t_k) = \boldsymbol{C}\boldsymbol{p}(t_k)P_{tot} \tag{22}$$

where $P_{\text{tot}} = \sum_{i=1}^{N} P_i$ and $\boldsymbol{C} = [c_1 \quad c_2 \quad \dots \quad c_n]$. In the limit when there is no load control, that is, $\mu_{ij}(t_k) = 0$, it can be seen that the aggregate load power $P(t_k)$ remains unchanging at the "nominal power" P_{tot}. The change in the aggregate load power between times t_k and t_{k+1} under load control can be represented as

$$y(t_k) = \boldsymbol{C}\left[\boldsymbol{p}(t_{k+1}) - \boldsymbol{p}(t_k)\right]P_{\text{tot}} \tag{23}$$

The switching probabilities should be derived so as to match the desired power modulation of the aggregate load given by $u_i(t_k)$ in (8) which yields

$$y(t_k) = \boldsymbol{C}\left[\boldsymbol{p}(t_{k+1}) - \boldsymbol{p}(t_k)\right]P_{\text{tot}} = u_i = k_i(\omega_i - \omega_i^0) \tag{24}$$

The above equation could have more than one solution if there are not additional constraints regarding the switching between different operating states. Therefore, when it comes to a specific type of controllable loads, additional switching constraints have to be added in order to solve for the forced switching probability. Otherwise, optimization problems can be formulated in order to minimize certain objectives such as the number of switching for each controllable load within each market clearing period.

2.3.2 Markov-chain model for HVACs and water heaters

In this section, Markov Chain models will be developed for specific class of TCLs including air-conditioners/heat pumps, water heaters, refrigerators and clothes dryers. An HVAC can be modeled using four operating states: ON, OFF, ON-LOCKED, and OFF-LOCKED. It is assumed that if the load switches to the locked states (ON-LOCKED or OFF-LOCKED), then it will stay in the locked states for the rest of the control period. The natural state switching within each control period is ignored and only forced switching is considered. The forced transition between groups of different operating states is depicted in Figure 1, where μ_1 denotes the forced switching probability from ON to OFF-LOCKED, and μ_0 denotes the forced switching probability from OFF to ON-LOCKED. Let $p_{\text{ON}}(t_k)$, $p_{\text{OFF}}(t_k)$, $p_{\text{ONLCK}}(t_k)$ and $p_{\text{OFFLCK}}(t_k)$ denote the percentages of the loads that are ON, OFF, ON-LOCKED and OFF-LOCKED, respectively, at time t_k.

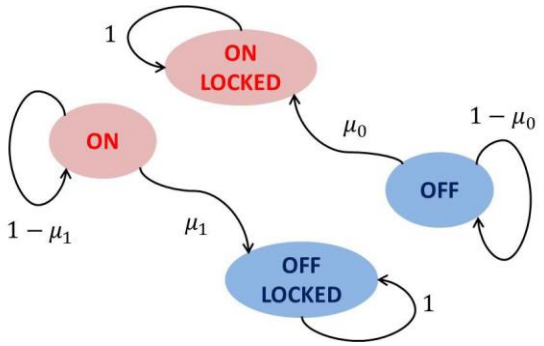

Figure 1 State transition diagram for a population of HVACs

The state transition matrix defined in (21), corresponding to the state transition diagram shown in Figure 1, is given by the following,

$$\boldsymbol{p}(t_k)=\begin{bmatrix} p_{\mathrm{ON}}(t_k) \\ p_{\mathrm{OFFLCK}}(t_k) \\ p_{\mathrm{OFF}}(t_k) \\ p_{\mathrm{ONLCK}}(t_k) \end{bmatrix};\ \boldsymbol{A}(t_k)=\begin{bmatrix} 1-\mu_1(t_k) & 0 & 0 & 0 \\ \mu_1(t_k) & 1 & 0 & 0 \\ 0 & 0 & 1-\mu_0(t_k) & 0 \\ 0 & 0 & \mu_0(t_k) & 1 \end{bmatrix} \tag{25}$$

Furthermore, $\boldsymbol{A}(t_k)$ can be decomposed as follows,

$$\boldsymbol{A}(t_k)=\boldsymbol{I}+\boldsymbol{B}_0\mu_0(t_k)+\boldsymbol{B}_1\mu_1(t_k) \tag{26}$$

where

$$\boldsymbol{B}_o=\begin{bmatrix} 0 & 0 & 0 & 0 \\ 0 & 0 & 0 & 0 \\ 0 & 0 & -1 & 0 \\ 0 & 0 & 1 & 0 \end{bmatrix};\boldsymbol{B}_1=\begin{bmatrix} -1 & 0 & 0 & 0 \\ 1 & 0 & 0 & 0 \\ 0 & 0 & 0 & 0 \\ 0 & 0 & 0 & 0 \end{bmatrix} \tag{27}$$

Water heaters can be modeled using two operating states: ON and OFF. Once again, the natural state switching within each control period is ignored and only forced switching is considered. The forced transition between groups of different operating states is depicted in Figure 2.

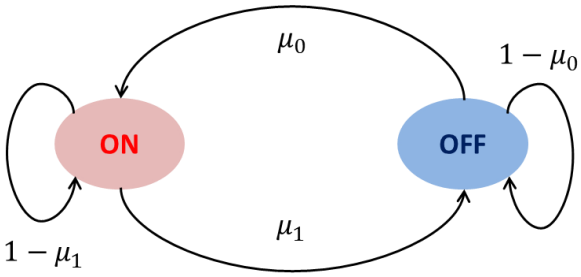

Figure 2 State transition diagram for a population of water heaters

The transition matrix corresponding to the state transition diagram shown in Figure 2 is given by,

$$\boldsymbol{p}(t_k)=\begin{bmatrix} p_{\mathrm{ON}}(t_k) \\ p_{\mathrm{OFF}}(t_k) \end{bmatrix};\ \boldsymbol{A}(t_k)=\begin{bmatrix} 1-\mu_1(t_k) & \mu_1(t_k) \\ \mu_0(t_k) & 1-\mu_0(t_k) \end{bmatrix} \tag{28}$$

Using the decomposition for $\boldsymbol{A}(t_k)$ given in (26), the following is obtained,

$$\boldsymbol{B}_o=\begin{bmatrix} 0 & 0 \\ 1 & 1 \end{bmatrix};\boldsymbol{B}_1=\begin{bmatrix} -1 & 1 \\ 0 & 0 \end{bmatrix} \tag{29}$$

For both HVACs and water heaters, the deviation of the actual aggregate load power from the nominal power during the control period can be determined as,

$$y(t_k) = \boldsymbol{C}\left[\boldsymbol{p}(t_{k+1}) - \boldsymbol{p}(0)\right]P_{tot} = \boldsymbol{C}\left[\boldsymbol{A}_{\Pi}(t_k) - \boldsymbol{p}(0)\right]P_{tot} \tag{30}$$

where $\boldsymbol{A}_{\Pi}(t_k) = \boldsymbol{A}(t_k)\boldsymbol{A}(t_{k-1})\cdots\boldsymbol{A}(0)$, $\boldsymbol{C} = [1 \quad 0 \quad 0 \quad 1]$ for HVACs and $\boldsymbol{C} = [1 \quad 0]$ for water heaters. Thus, the forced switching probabilities $\mu_0(t_k)$ and $\mu_1(t_k)$ can be calculated by requiring $y(t_k)$ to match the desired power modulation $u(t_k)$ for each device control period of length $\Delta t_d = t_{k+1} - t_k$.

2.4 Overall implementation of hierarchical demand-side frequency control algorithm

In this section, the decision making process at each layer in the hierarchical demand-side frequency control algorithm is summarized in the form of the following algorithm.

Step 1: At the beginning of each control period, each device reports its operating state and power to the supervisory controller. After collecting all the information, the supervisory level controller sends $p(0)$ and P_{tot} to each device. In this way, each device can initialize a local copy of the Markov-Chain model to predict the aggregate load response.

Step 2: At each control time step, every device receives the desired power modulation signal $u(t_k)$ from the supervisory layer. In order to calculate the switching probabilities $\mu_0(t_k)$ and $\mu_1(t_k)$ locally, each device needs to compute the following expression,

$$a(t_k)\mu_0(t_k) + b(t_k)\mu_1(t_k) = c(t_k) \tag{31}$$

where

$$\begin{aligned}
a(t_k) &= \begin{cases} \boldsymbol{C}\mathrm{B}_o\boldsymbol{p}(0) & \text{if } t_k = 0 \\ \boldsymbol{C}\mathrm{B}_o\mathrm{A}_{\Pi}(t_{k-1})\boldsymbol{p}(0) & \text{if } t_k > 0 \end{cases} \\
b(t_k) &= \begin{cases} \boldsymbol{C}\mathrm{B}_1\boldsymbol{p}(0) & \text{if } t_k = 0 \\ \boldsymbol{C}\mathrm{B}_1\mathrm{A}_{\Pi}(t_{k-1})\boldsymbol{p}(0) & \text{if } t_k > 0 \end{cases} \\
c(t_k) &= \begin{cases} \dfrac{1}{P_{tot}}u(t_k) & \text{if } t_k = 0 \\ \dfrac{1}{P_{tot}}u(t_k) + \boldsymbol{C}\left[\boldsymbol{I} - \mathrm{A}_{\Pi}(t_{k-1})\right]\boldsymbol{p}(0) & \text{if } t_k > 0 \end{cases}
\end{aligned} \tag{32}$$

Step 3: With the goal of minimizing the total number of times the devices switch their operating states, each device then solves for the forced switching probabilities given by the following.

$$\begin{aligned}
\mu_0(t_k) &= \begin{cases} \dfrac{c(t_k)}{a(t_k)} & \text{if } u(t_k) > u(t_{k-1}) \\ 0 & \text{otherwise} \end{cases} \\
\mu_1(t_k) &= \begin{cases} \dfrac{c(t_k)}{b(t_k)} & \text{if } u(t_k) < u(t_{k-1}) \\ 0 & \text{otherwise} \end{cases}
\end{aligned} \tag{33}$$

Step 4: Then each device switches its operating state according to the above forced switching probabilities so that the actual deviation of aggregate load power from the nominal power will match the desired power modulation for every device control period.

3.0 Validation of modified control strategy on large-scale systems

Large power system interconnection studies are typically performed by utility and research engineers with commercial software, like Siemens PTI PSS/E [21], GE PSLF [22], and more recently, PowerWorld Simulator [20]. These software tools maintain the algorithm and standard models of particular elements (such as power lines, synchronous machines, governors), so that engineers can draw conclusions using the same base models.

Utilities and interconnection coordinators, such as the WECC, update and manage the databases for their models. Most of the models are standard and are available in commercial software libraries. New proposed models and control strategies, like the hierarchical demand-side frequency control proposed in this report, need to be incorporated in commercial tools as user-defined models. These models remain that way until the model becomes more widely used, after which it is incorporated into the standard libraries of the software packages. This section describes the implementation of the model for the hierarchical demand-side frequency control on the WECC interconnection model. A user-defined model was developed to interact with the rest of the model of the WECC system in the PowerWorld Simulator software. Simulation results and sensitivity studies demonstrate the effect of the hierarchical demand-side frequency control on the WECC system.

3.1 Implementation of hierarchical demand-side frequency control in PowerWorld

Dynamic simulations capture electromechanical dynamics of large power system interconnections. The dynamic models are composed of individual dynamic device models, such as synchronous generators with their controls (e.g., automatic voltage regulators and governors) coupled with a model of the transmission network. Other dynamic device models may include electric motors, high voltage dc transmission systems, and dynamic load models. The dynamic device models are represented by differential equations and the transmission network is represented by algebraic equations. The full model is a system of differential-algebraic equations. This system of equations is solved using numerical integration to obtain the trajectories of the system states from which trajectories of electrical variables, such as power flows and electrical frequency, are derived.

In large-scale interconnection models, the load represents high voltage substations of tens to hundreds of MW. This is an aggregated representation of many end-use loads and distribution networks connected to those substations. The representation of such models can either be static, such as the ZIP model (portions of constant impedance, constant current, and constant current) or dynamic, such as motor load models. There is currently work in progress in WECC working groups to incorporate more detailed composite loads models (with various types of motors, electronic loads, static loads, and an equivalent of the distribution network and substation transformers). However, this new model has not been used in this project and it is under consideration for future work.

To represent the hierarchical demand-side frequency control, a new dynamic device model was implemented. This dynamic device model has to interface with the network model that will interconnect all of the dynamic device models in the system. PowerWorld has incorporated an interface in their

transient stability application model that allows creating models in Visual Studio C++ 2010 as a DLL. The DLL communicates between the differential equations in the user defined models and the network models in PowerWorld.

The user defined model for the hierarchical demand-side frequency control implements the following elements:

- Load dynamic behavior which is captured by the different versions of Markov chains described in Section 2.3.2 , representing dynamic behavior of populations of end use water heaters and HVACs
- Frequency controller that affects the water heaters and HVACs populations, as discussed in Section 2.4
- Electric load model that is modified by the previous two elements

In the current implementation, the electric load model which is a static ZIP load model. Using the ZIP static load model could be an acceptable approximation to represent water heater loads. However it is a crude approximation for HVAC loads, where the motor dynamics should be included.

Additionally the effect of the distribution network between the high voltage substation and the end-use load should be considered. For example, when resistive water heater loads at the end-use change, the reactive power consumption of the distribution networks change, causing a change in the reactive power load at the substation level. As a first approximation, this effect was captured in the current model by modifying the reactive power proportionally to the changes in active power load due to the action of the hierarchical demand-side frequency control.

Additional work needs to be done to improve the limitations mentioned above of the electrical characteristics of the current model implementation. As mentioned before, one step towards this direction could be to implement the hierarchical demand-side frequency control model in the new detailed composite load model being developed by WECC working group. Additional steps to gain insight on this problem could include using interfaced transmission models and distribution models such as PowerWorld and GridLAB-D, which is an open-source distribution simulation tool.

3.2 WECC test scenarios

WECC 2014 (high-load summer) and 2022 (low-load winter) cases were used to test the hierarchical demand-side frequency control. This section provides a summary of the WECC system model and the scenarios of controllable loads in terms of amount and location. The WECC system has about 20,000 buses, 3,900 generators, 16,000 transmission lines, and 10,800 loads. As shown in Figure 3, the WECC system covers the western parts of the United States, Canada, and the northern portion of Baja California, Mexico. The 2014 high-load summer case has a total load of about 167,000 MW, and the 2022 low-load winter case has a total load of about 109,000 MW.

The green circles in Figure 3 indicate the areas where the controllable loads were placed. The electrical frequency at one bus at each of these areas was monitored for the purposes of reporting results. Three interties in the system (blue circles in Figure 3) were monitored also for result reporting purposes.

140 loads in total were controlled representing 40,100 MW. The largest loads of the 12 areas, indicated in the green circles in Figure 3, were chosen as controllable. This distribution resulted in 80% of controllable load is located in the southern part of the WECC system, and 20% of the controllable load is located in the rest of the system.

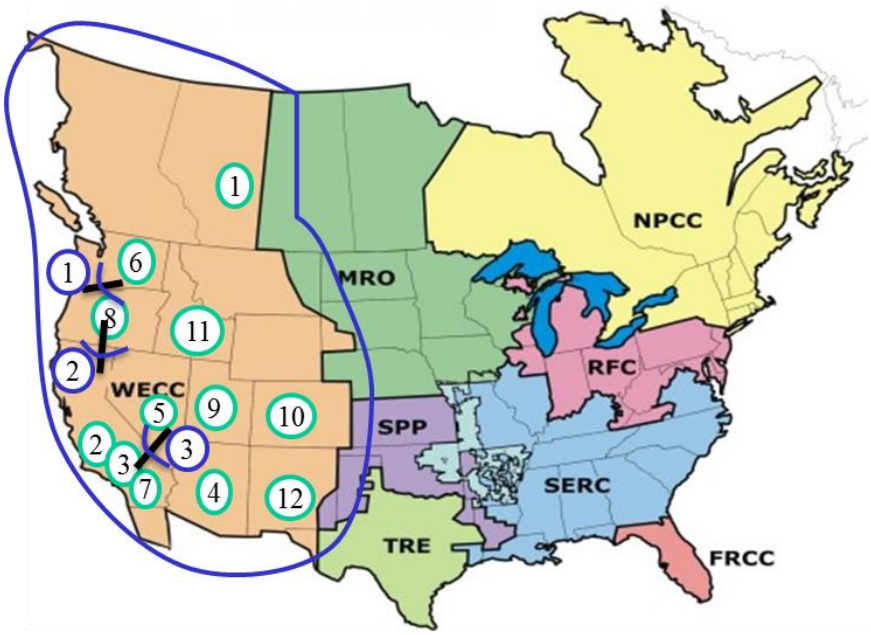

Figure 3 Geographical location of WECC system, areas where controllable loads where located (green circles), and monitored interties (blue circles)

3.3 Simulation results

The hierarchical demand-side frequency control was tested in four simulation cases in the WECC system: i) comparison with and without load control, ii) sensitivities to control gain parameters, iii) location of controllable load, and iv) type of end-use devices being controlled. These simulation cases are discussed in the following subsections.

3.3.1 Case 1: With and without load control

In this section, for the WECC high-load summer 2014 scenario, the cases with the proposed hierarchical frequency responsive load control is compared to the case without load control. It can be seen from Figure 4, that the proposed load controller showed improved frequency recovery in terms of steady state error and maximum frequency deviation as compared to the case without load control.

The effect of load control on the power flow of intertie 2 (one of the north-south tie-lines), is shown in Figure 5. The intertie power flow increases after the event because there is more responsive generation in the north in the summer. With higher concentration of controllable loads in the south of the WECC

(80% of controllable loads located in the southern WECC), the intertie power flow is lower than the case without load control. This shows a benefit of load control complementing the response of generator control. Overall, these results indicate that load control can potentially increase the overall reserve for primary frequency control and complement the generation side control.

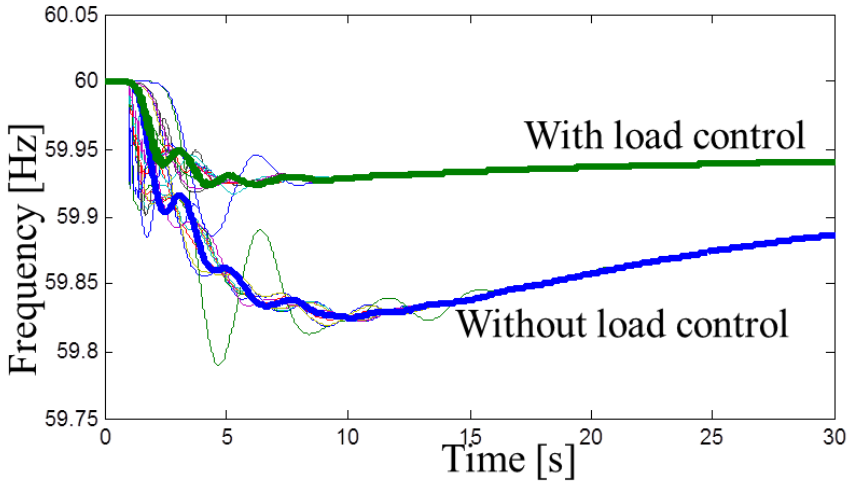

Figure 4 Electrical frequency one bus of each of the 12 areas where the controllable loads were placed for the cases with and without load control

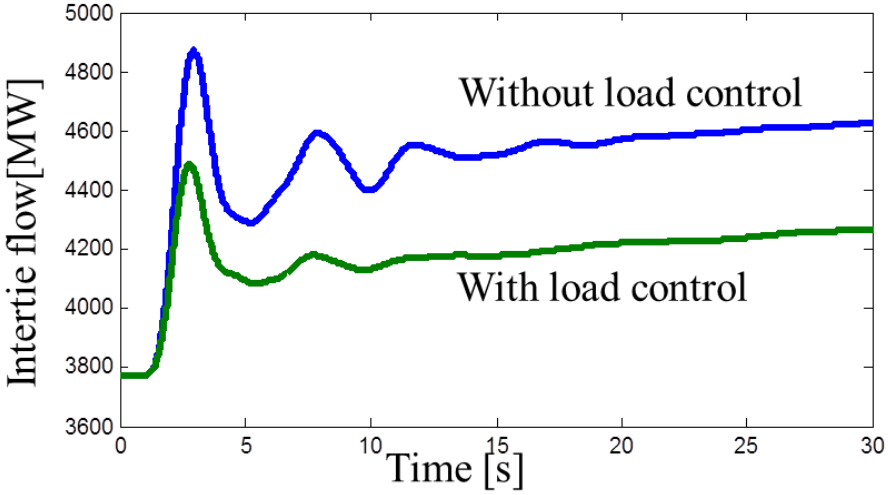

Figure 5 Intertie flow for the cases with and without load control

3.3.2 Case 2: Sensitivity to control gain parameters

This section presents sensitivity studies to controller gain values when there is high availability of controllable load in the WECC system. The high summer 2014 and low winter 2022 scenarios are used in the studies. Water heater loads were used in these tests system. The control gain and penetration of controllable loads were adjusted such that 1%, 2.5%, 5.6% and 10% of WECC load responds to the frequency event. It is important to note that even if the penetration or availability of controllable load is higher than 10%, the control gain can be adjusted at to achieve any of the % of the responsive loads

studied in this section. Figure 6 shows the results of the WECC electric frequency at one bus for the different percentages of responsive load. It can be observed that high penetration of controllable loads, combined with high values of controller gain, can reduce the frequency deviation. A "chattering" in the response is observed for high gain values. This corresponds to the discrete implementation of the load model and controller. The question of whether this "chattering" effect could appear in the actual implementation is a matter of future research.

An important feature of the developed controller is that the system operator can choose to adapt the value of the gain from the supervisory control level to adapt to the available controllable load resources, changing operating conditions, and to achieve coordination with other available resources providing primary frequency control. Also, it can be seen from Figure 7, which is the future WECC 2022 scenario, that selecting 1% of responsive load yields a comparable performance to the WECC 2014 scenario.

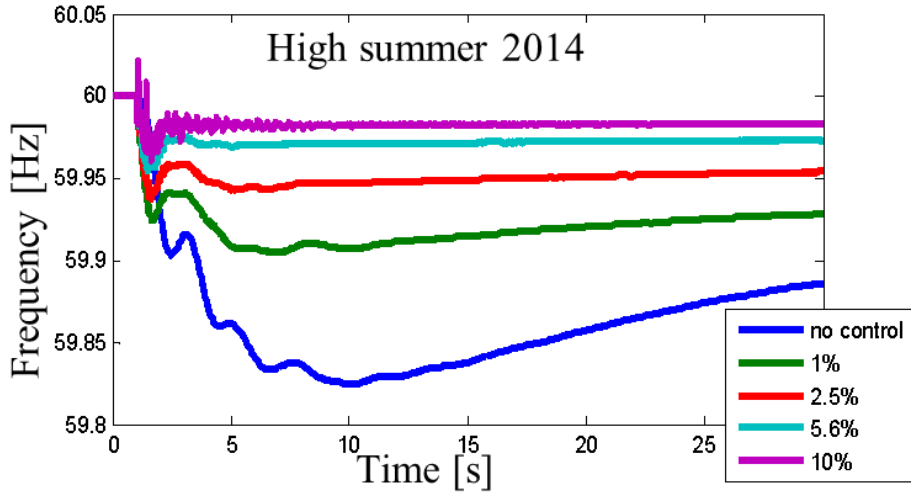

Figure 6: WECC electric frequency at one bus for the different percentages of responsive load

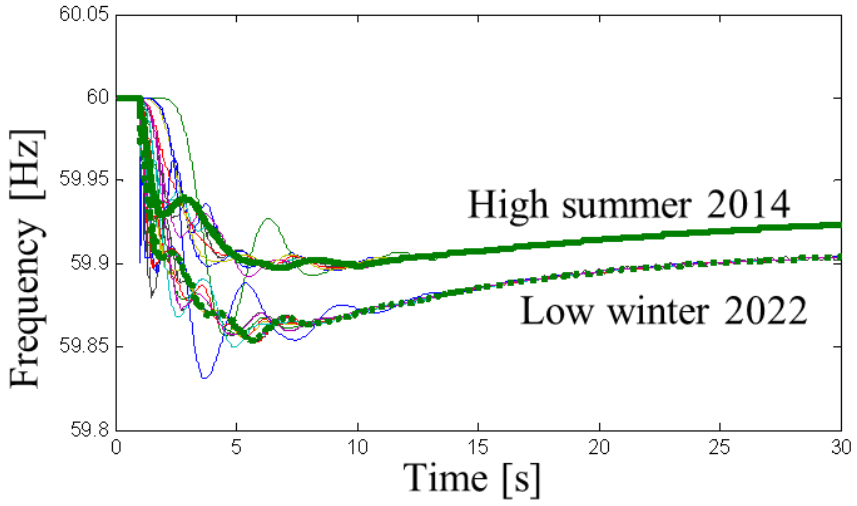

Figure 7: WECC electric frequency at several buses for 1% of responsive load

3.3.3 Case 3: Sensitivity to location of controllable loads

In order to study the sensitivity of location on the performance of the frequency responsive controllable loads, three scenarios are studied: a) all the controllable loads are concentrated in the south, b) all the controllable loads are deployed in the northwest and c) controllable loads are distributed across the 12 areas under consideration. In order to simulate a contingency event, a large generation trip is simulated in the south of the system. The system frequency and intertie power flows without load control and with load control in different locations are given in Figure 8 and Figure 9 respectively.

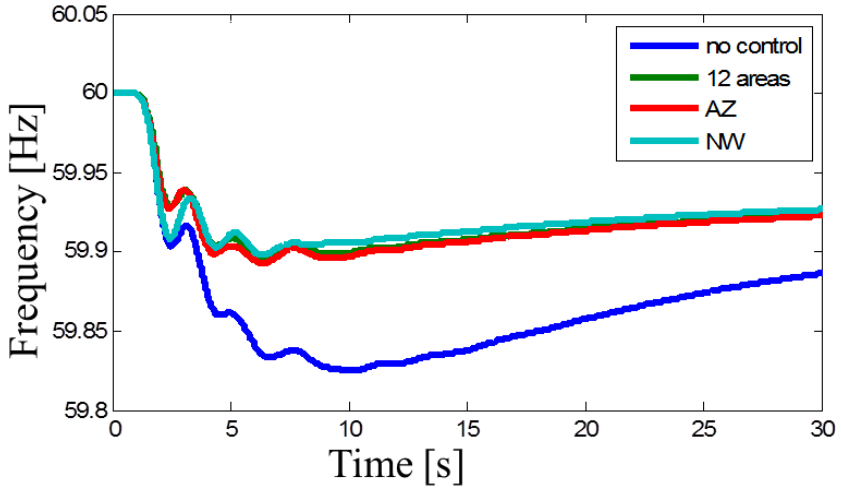

Figure 8 System frequency performance under different locations of controllable loads

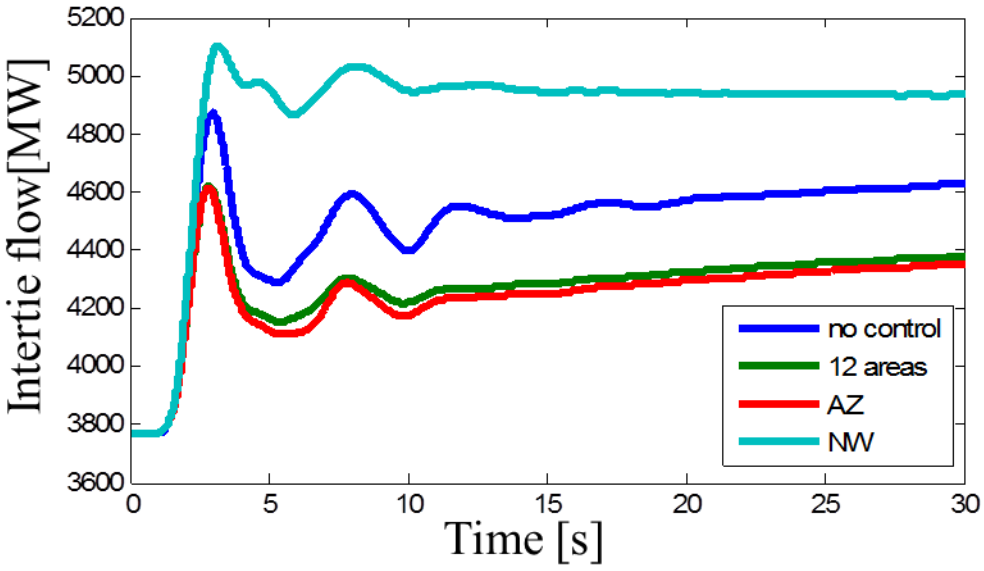

Figure 9 Intertie power flow under different locations of controllable loads

As mentioned previously in Section 3.3.1, the proposed load controller showed improved frequency recovery in terms of steady state error and maximum frequency deviation as compared to the case without load control. It also appears that system frequency performance is relatively insensitive to where the

controllable loads are located. On the other hand, the intertie power flow response depends on relative location of disturbance and load/generation providing primary frequency control. An overall conclusion that could be made is that load control could be used as additional resource in areas with lack of generation, for example in the south of WECC during the summer.

3.3.4 Case 4: Sensitivity to type of controllable load

The focus of this section is to study the sensitivity of the proposed load control strategy to the type of end-use loads that are being controlled. In particular, the behavior of a population of water heaters was compared to the behavior of a population of HVACs. The objective of these simulations is to show the effect of the lockout time characteristic of the HVAC system as compared to water heaters that do not have this limitation. Recall from Section 2.3.2 that the lockout time characteristic maintains an HVAC device in OFF state for 2 minutes before the thermostat or any other controller can turn it back ON.

To study the effects of the lockout time in the population of HVACs, the sensitivity to the percentage of HVAC that are able to turn on, when the frequency recovers after an event, was studied. In other words, consider the HVAC population dynamics as two groups of HVAC loads: a) the first group is initially (before the frequency event) in the ON state and gets turned OFF when the frequency drops, after which this group gets locked out and cannot be turned back on by the load controller; b) the second group is initially (before the frequency event) in OFF state and will be able to be turned ON by the controller when the frequency recovers. The sensitivity in this section considers the percentage of HVAC that are in group b), and it also compares the performance to the case when all the controlled loads are composed of water heaters. The cases studied in this section are:

- Case “water heaters” (as denoted in the figures of this section): all controllable loads are water heaters; there is no lockout time, and the water heaters can be turned back on when the frequency recovers

- Case “HVAC 0% able to turn on”; all controllable load are HVAC; this case has no HVACs in group b) (group of HVAC initially OFF that can later be turned ON by the controller when the frequency recovers), meaning that, after the frequency event, there will be no HVACs that are able to be turned ON by the controller ON when the frequency recovers

- Case “HVAC 2.5% able to turn on”; all controllable load are HVAC; this case has 2.5% of all HVACs in group b) (group of HVAC initially OFF that can later be turned ON by the controller when the frequency recovers); meaning that, after the frequency event, there will be 2.5% HVACs that are able to be turned ON by the controller when the frequency recovers

- Case “HVAC 5% able to turn on”; all controllable load are HVAC; this case has no HVACs in group b) (group of HVAC initially OFF that can later be turned ON by the controller when the frequency recovers), meaning that, after the frequency event, there will be 5% HVACs that are able to be turned ON by the controller when the frequency recovers

The frequency performance results and total power at a bus are shown in Figure 10 and Figure 11 respectively. It can be seen that the response for the case “HVAC 5% able to turn on” is very similar to the response for the case “water heaters.” This is because, for this simulation, 5% of HVAC that are able to be turned ON by the controller when the frequency recovers is enough to eliminate the shortcomings of

lockout time. Hence the full HVAC population, despite the lockout time of individual HVACs, behaves similar to a population of water heaters without lockout time in individuals. The lockout effect in HVACs starts to be more evident in the population in the cases of "HVAC 2.5% able to turn on" and "HVAC 0% able to turn on," as shown in the figures. Figure 11 sows the effect of lockout in HVAC populations in the load response at a substation bus. The case "HVAC 0% able to turn on" results most impacted by lockout times because the controller has no devices to turn back ON to follow the frequency recovery. In Figure 10, it can be seen that the effect of the lockout (cases "HVAC 2.5% able to turn on" and "HVAC 0% able to turn on") causes the frequency to recover to values closer than 60Hz. Although getting closer to 60Hz seems, at first sight, an advantage, it is not so. It is important to note that this apparent better recovery is not the response dictated by the controller, and depending on the particular event, these uncontrolled response could cause undesired effects, such as making the frequency grow above 60Hz. Such situation deserves further study.

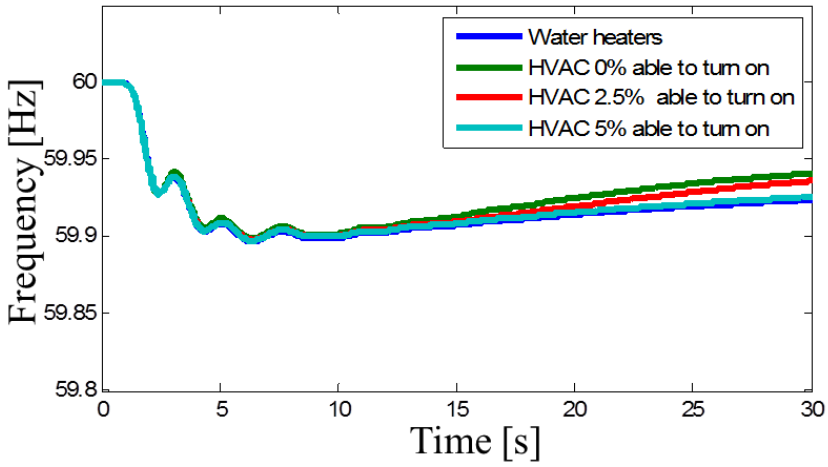

Figure 10 System frequency performance using different types of controllable end-use loads

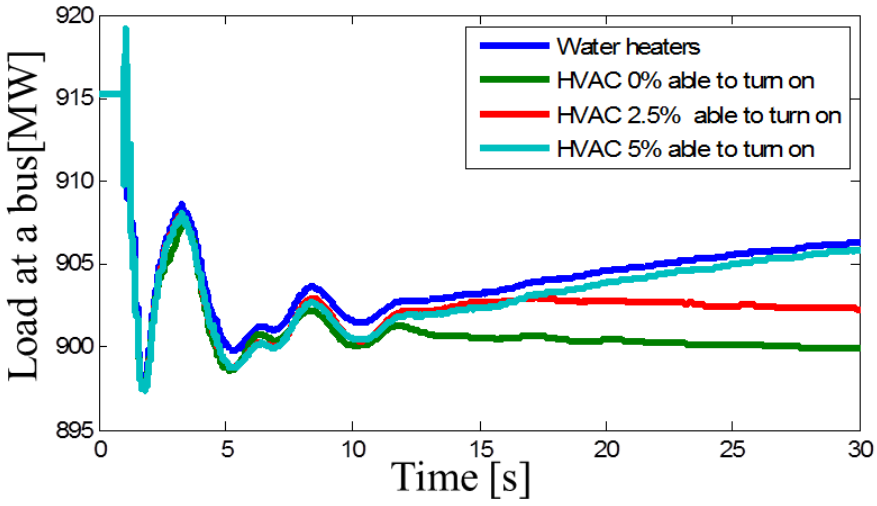

Figure 11 Total power at a bus using different types of controllable end-use loads

The results indicate that the implemented load population model and controller is sensitive to the dynamics of different types of end-use loads (i.e., HVAC vs. water heaters). The sensitivity study of this section shows that the type of loads could affect control performance, depending on the characteristics of the population in that particular substation. The system-wide effect of the different type of loads requires additional study.

3.4 Summary and conclusions of validation tests

The load models and control strategy were implemented and tested on the WECC 2014 and 2022 scenarios, with the PowerWorld simulation software. This simulation allows gaining insight on system effects of the developed load control strategy in a large scale interconnection. The tests confirmed how the load control strategy can bring about several benefits. Compared to the case without load control, the simulations of the load controller showed improved frequency recovery in terms of steady state error and maximum frequency deviation. This demonstrated that loads controlled with the implemented strategy can be used to complement frequency responsive generation.

The simulations showed that the response of intertie power flows depends on relative location of disturbance and responsive load and generation. This brings an opportunity where load control could be used as additional resource in areas with lack of generation (e.g., southern WECC in summer).

The implemented load population model and controller captures the dynamics of different types of end-use loads (i.e., HVAC vs. water heaters). The sensitivity study of this section shows that the type of loads could affect control performance, depending on the characteristics of the population in that particular substation. The system wide effect of the different type of loads deserves additional study.

The control gain can be adapted, by the system operator from the supervisory control level, based on the available controllable load resources, changing operating conditions, and to achieve coordination with other available resources providing primary frequency control. The simulations on this section showed that the response is robust for a wide range of load penetration and control gains in the WECC system, so this gain adaptation does not need to happen often.

4.0 Enhanced Grid Friendly Appliance design

The promise of autonomous, Grid Friendly response by smart appliances in the form of under-frequency load shedding was demonstrated in the GridWise Olympic Peninsula Demonstration in [8] and [9]. Grid Friendly™ Appliance controllers in the GridWise Olympic Peninsula provided autonomous under-frequency load shedding in dryers and water heaters. Each controller monitored the power grid frequency signal and requested that electrical load be shed by its appliance whenever electric power grid frequency fell below a unique and randomly chose threshold between 59.95 Hz and 59.985 Hz. The controllers and their appliances responded reliably to each shallow under-frequency event, which was an average of one event per day and shed their loads for the durations of these events.

Autonomous responses are critical for many reliability purposes where there may not be time to communicate needed actions through wide-area network. Appliance and equipment manufacturers are rapidly moving toward mass production of devices with smart grid capabilities that can be leveraged for this purpose. However, utilities and balancing authorities have been hesitant to support such deployments, primarily because the response of fleets of such devices has not been fully integrated with their control schemes for grid stability. The report presented in [10] studied the impacts of a population of frequency responsive GFAs on the bulk power system frequency stability through extensive simulation studies, where the GFAs are designed as demonstration units and modeled individually as water heaters.

In [10], several important factors regarding the design of the GFA controller and the deployment of GFAs were carefully examined. In particular, the performance of the GFAs was evaluated in terms of certain key parameters, such as level of GFA penetration, geographical location, and response. Their effects on the overall system response were analyzed and classified into the following findings:

- The geographical distribution of GFA loads within the system has obvious influence on the impacts of frequency responsive GFAs on the bulk power system. The extensive simulation studies suggested that it is better to have all the GFAs deployed in the proximity of the location where the under-frequency events have been caused. However, it is impossible in practice to know beforehand the location for the under-frequency events. Thus, the simulation studies alternatively suggested that it be preferable to have GFAs evenly distributed within the system. The fulfillment of the even geographical distribution will require the coordination among system operators from different areas. This is beyond the scope of the technical design of the GFA controller.

- The response time of the GFA controller, that is, the time constant of the low-pass filter for frequency measurement, is one of the crucial design parameters that can directly affect the frequency response of the bulk power system. In general, the shorter the response time, the better the system response. However, the problem with smaller response times is that GFAs could respond to false inputs and noise. Thus, it requires the engineering judgment to determine the response time of the GFA control. In practice, the appropriate selection can be done by analyzing the frequency characteristics of historic under-frequency events.

- The penetration level of online GFAs (i.e., the GFAS that are currently ON) within the system turns out to have the most significant influence on the frequency response of the bulk power system. As suggested by the extensive simulation results, the system tends to have

large transients as the penetration level of online GFAs increases. This is not desired for practical system operation since large transients could potentially drive the system to instability. Hence, it brings up the question about how many online GFAs should actually respond to the under-frequency events. However, due to the autonomy of the GFA controller, all the GFAs that are currently ON in the system will respond regardless of possible negative consequences of the aggregated effect. It is necessary to coordinate the autonomous response of online GFAs from different geographical locations up to certain extent so that the negative consequences can be avoided.

In this section, the impacts of frequency responsive GFAs on bulk power system are analyzed further by examining the curtailing frequency threshold, which is another important design parameter of the GFA controller. When the actual distribution of the pre-determined thresholds is biased, it could potentially impact the system response negatively. Based on the performed analysis, a supervisor is introduced at each distribution feeder to systematically monitor the state of the system. Whenever it is necessary, the supervisor can modify the thresholds of all the supervised GFAs in such a way that their autonomous responses will be coordinated to avoid any potential negative effects. Furthermore, the introduced supervisor also offers a solution to the issue related to the high penetration level of online GFAs in the system as identified in [10]. The cause of this issue is because the range of curtailing frequency thresholds is fixed regardless of the penetration level of online GFAs. In this case, there will be more online GFAs to be triggered than needed when the penetration level is high, which is definitely detrimental to the system response. Therefore, it is necessary make the range of the thresholds adaptive to the penetration level of online GFAs in the system. When the penetration level of online GFAs increases, the range of the thresholds should be enlarged and the thresholds of online GFAs should be re-sampled from this enlarged range. This can be achieved by the introduced supervisors. They will first determine the current penetration level through information discovery by communicating with their neighbors, and then communicate the new range to supervised GFAs and require them to re-sample the threshold.

4.1 GFA control logic

The GFA controller developed at Pacific Northwest National Lab (PNNL) is a small electronic device that resides within the appliances. It is configured to observe the AC voltage signal available to the appliances at their wall outlets, autonomously detect under-frequency events, and alter the operating mode of the appliances to help the power grid, provided their current operating mode can be changed. As described in [10], four operating modes have been defined for each individual GFA: active, triggered, curtailed, and released. The GFA control logic is schematically depicted in Figure 12.

In the *active* operating mode, the individual GFA evolves based on its internal dynamics, turning ON or OFF according to its predefined control logic. Once the GFA controller detects the grid frequency falls below the threshold f_{t_th}, the GFA changes its operating mode from *active* to *triggered*. It remains in this mode for a time period t_{b_c} (time before curtailment) as long as the grid frequency does not return above f_{t_th} within a time period t_{d_c} (curtailment time delay). The time period of t_{d_c} is actually defined by the response time of the low-pass digital filter in charge of smoothing the frequency measurements in order to avoid reactions to unrealistic data and noise. If the under-frequency event persists longer than the response time t_{d_c} of the GFA controller, the device shuts down and switches from *triggered* to *curtailed*. Once the grid frequency rises above threshold f_{r_th}, where $f_{r\_th}>f_{t\_th}$, the GFA moves into the *released* operating mode. It remains there for a time period t_{b_a} (time before activation) provided the grid

frequency stays above f_{r_th} at least a time interval equal to t_{d_a} (activation time delay). The time period of t_{d_a} is designed in order to minimize the rebound effect when all the GFAs would turn on at the same time. At the end of the period of t_{d_a}, the GFA switches back to *active* mode, and follows its nominal internal dynamics.

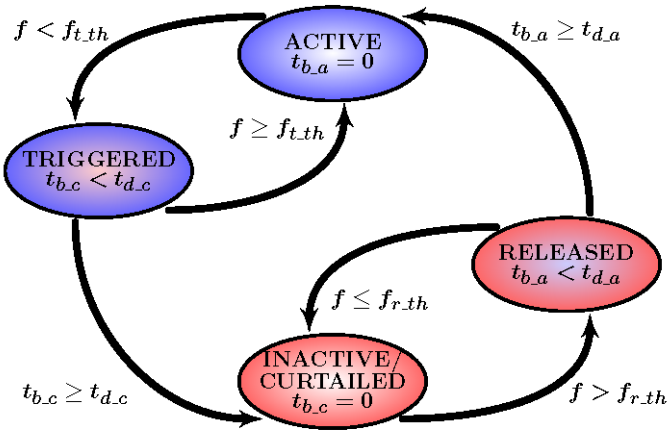

Figure 12 Schematics of GFA control logic

The turning-off time delay of each unit (i.e., the response time) is the effect of the response time of the low-pass digital filter in charge of smoothing the frequency measurements in order to avoid reactions to unrealistic data and noise. The turning-on delay (the time interval between the moment the frequency has recovered and the moment the device is free to act according to its own dynamics) is designed to minimize the rebound effect. That means that the controlled devices will not turn on until the grid has been stabilized. In the subsequent study involving water heaters with GFA controllers, the turning-off time delay of each unit is selected to be 0.4 seconds as specified in [8] for the hardware implementation. The turning-on delay is randomly chosen between 2 and 3 minutes. Based on the historical data analysis described in [17], the range of curtailing frequency thresholds for GFAs is set to be between 59.95 Hz and 59.985 Hz as specified in [10]. Similarly, the range of releasing frequency thresholds is set to be between 59.995 Hz and 59.999 Hz. All the curtailing and releasing frequency thresholds are sampled uniformly in the above defined ranges.

4.2 Curtailing frequency threshold

In the current design of the GFA controller, the range of curtailing frequency thresholds is determined offline to be between 59.95 Hz and 59.985 Hz. The exclusion of any frequencies between 59.985 Hz and 60 Hz from being selected as thresholds is to impose a deadband for the GFA response. Otherwise, the GFAs with thresholds close to 60 Hz will suffer from frequent triggering that is disruptive to their normal operation. All the GFAs in the system will randomly select their curtailing frequency thresholds from the above range based on a uniform distribution and keep them fixed. The objective of such a probabilistic approach in determining the curtailing frequency thresholds is to expect the power reduction from online GFAs that are triggered when under-frequency events occur is proportional to the frequency deviation. Such a response is often referred to as droop-like response. However, as will be illustrated in the following analysis, the actual response is not always guaranteed to be droop-like. In order to easily visualize the aggregate response from online GFAs, the supply curve that describes the relationship

between the available power reduction and the frequency deviation at any time instant will be constructed. With the help of supply curve, the impact of the actual distribution of the curtailing frequency thresholds of online GFAs can also be easily identified.

In order for online GFAs to have a droop-like response, the desired relationship between the power reduction and the frequency deviation should be described by the supply curve as shown in Figure 13(a). In this desired case, the effect of deadband has been taken into account. Figure 13(b) shows an example of the actual distribution of the curtailing frequency thresholds and power ratings of online GFAs, whose corresponding supply curve will be given by Figure 13(a).

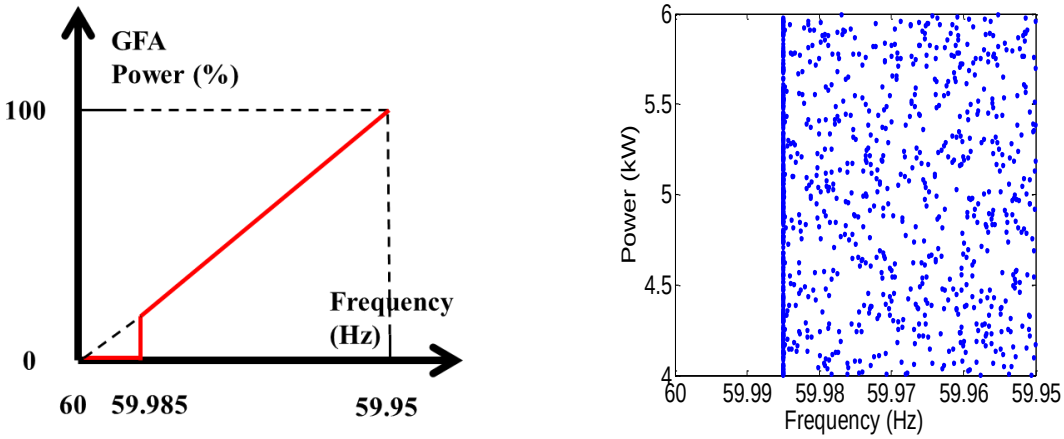

(a) (b)

Figure 13 Desired relationship between power reduction and frequency deviation

Since the curtailing frequency thresholds of all the GFAs are sampled from the range based a uniform distribution, it is very likely that the thresholds of online GFAs at any time instant are evenly distributed within the entire range, as shown in Figure 14(a). In this unbiased case, the supply curve will be given by Figure 14(b), which is different from the desired supply curve as shown in Figure 13(a). Thus, it is clear that the aggregate response of online GFAs will not be droop-like. When the frequency deviation is just below, but around 59.985 Hz, there will be noticeable difference in the system response between the desired and the unbiased cases. For the unbiased case, the system response will be similar to that without any GFAs in the system, because very few GFAs will be triggered due to the small frequency deviation. On the other hand, when the frequency deviation is large and beyond 59.95 Hz, the difference in the system response between the desired and the unbiased cases will become minor. This will be later confirmed by simulation studies.

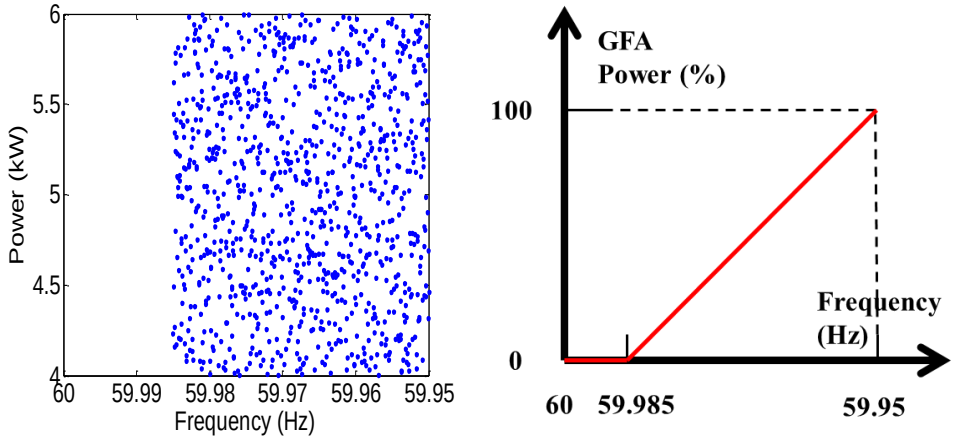

(a) (b)

Figure 14 Normal relationship between power reduction and frequency deviation

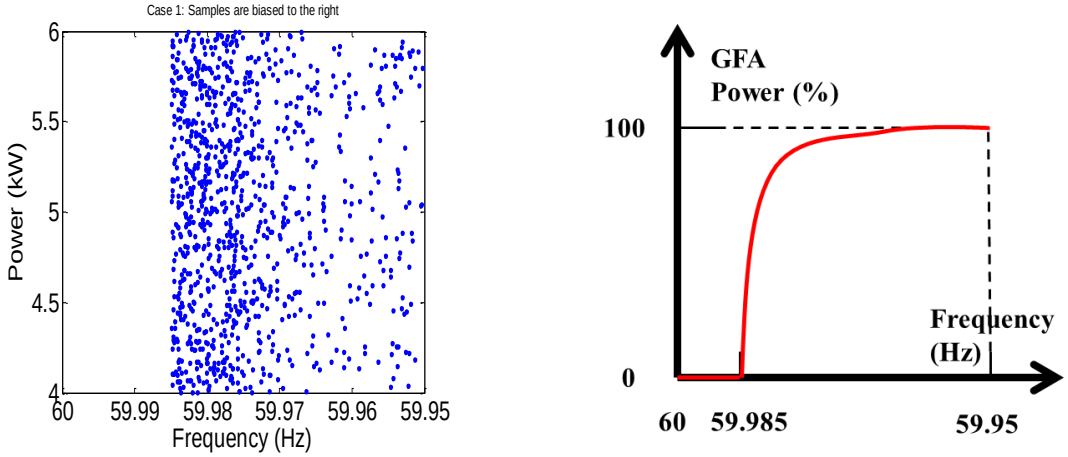

(a) (b)

Figure 15 Left-biased relationship between power reduction and frequency deviation

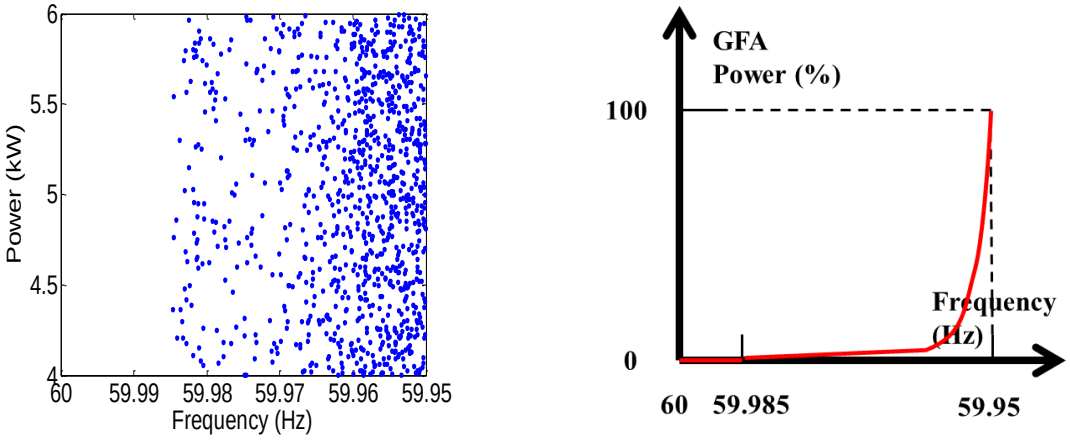

(a) (b)

Figure 16 Right-biased relationship between power reduction and frequency deviation

Although the thresholds of online GFAs are evenly distributed within the entire range, it is still possible the actual distribution is severely biased, as shown in Figure 15(a) and Figure 16(a). In these biased cases, the corresponding supply curves are shown in Figure 15(b) and Figure 16(b), respectively. When the frequency deviation is just below, but around 59.985 Hz, the response from online GFAs in the left-biased case could potentially make the system response worse. This would be due to excessive power reduction in the left-biased case, while there may not be any power reduction in the right-biased case. On the other hand, when the frequency deviation is large and beyond 59.95 Hz, the system response for both cases could be similar. Again, this will be confirmed by the simulation studies.

4.3 Comparative case studies

The test system used for the case studies is the IEEE 5-area, single-line, 16-machine, 86-transmission-line, and 68-bus test system available in [18]. The test system's parameters are taken from the data files that come with the Power System Toolbox (PST) distribution [19]. The IEEE 16-machine, 86-transmission-line, and 68-bus test system is shown in the single line diagram in Figure 17. Its configuration approximates the interconnection between the New England test system (NETS) and the New York power system (NYPS). NETS and NYPS are represented by generators G1 to G9 in area 4, and generators G10 to G13 in area 5, respectively. Generators G14 to G16 are equivalent aggregated generators modeling the 3 neighboring areas connected to NYPS. The total load in the whole system is 18,333.90 MW, with a distribution of 5,039.00 MW of demand in the NETS area (area number 4), and 7,800.95 MW in the NYPS area (area number 5). According to the steady-state power flow, NYPS imports some of the power generated in NETS. The GFAs in these studies are selected to be electric water heaters. The total load of online GFAs is 1,350 MW, which accounts for approximately 11% of total demand in areas 4 and 5. These online GFAs are evenly distributed among areas 4 and 5.

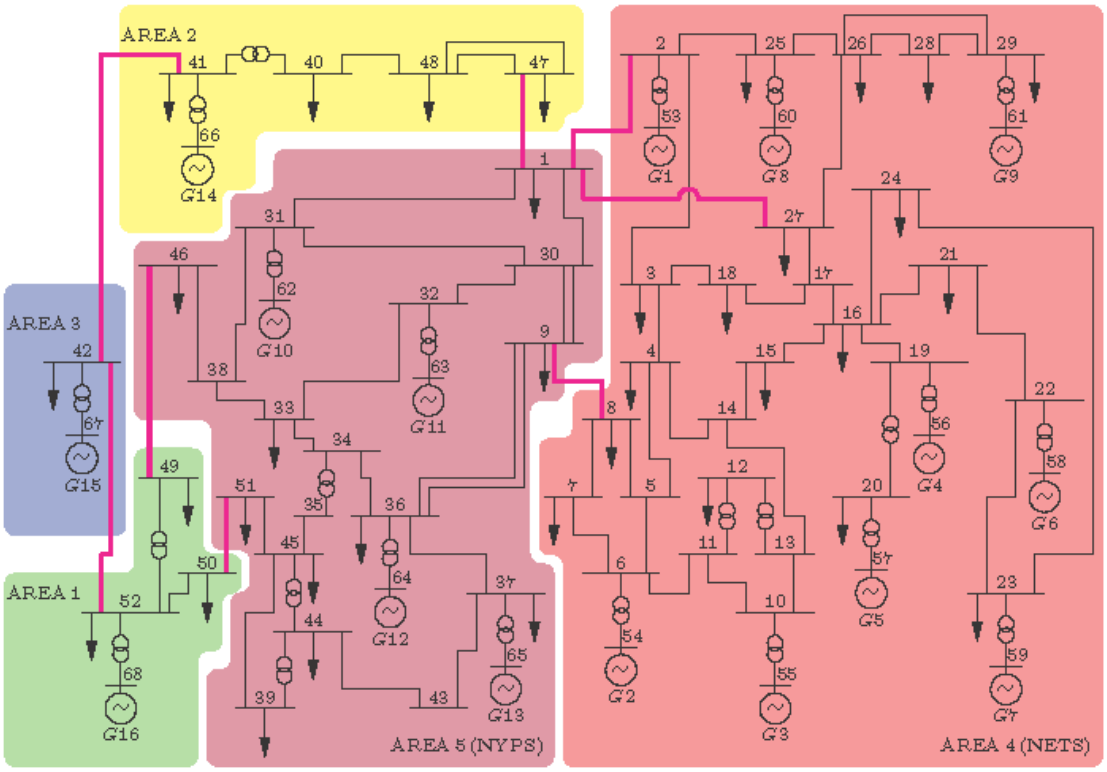

Figure 17 IEEE 5-area, 16-generator, 68-bus test system

Case I: In the first case study, the system responses are compared when the supply curves from online GFAs are different. Specifically, the four different supply curves as discussed in the previous section are tested. The under-frequency event in this case study is caused by the tripping of generator G1. Since the capacity of generator G1 is small, the resulting frequency deviation is within the range of 59.95 Hz and 59.985 Hz. Figure 18 shows the rotor speed responses of generator G5 in this case. Several observations can be made when the frequency deviation is small.

- The system response with the desired supply curve from online GFAs is greatly improved compared to the response without any GFAs. This demonstrates the contribution of GFAs to frequency protection during under-frequency events when the supply curve is desired.

- The system response with the unbiased supply curve from online GFAs is only improved slightly compared to the response without any GFAs. This indicates that the contribution of GFAs to frequency protection is very limited if the supply curve is unbiased. Since the supply curve from online GFAs is most likely unbiased, the current method of selecting curtailing frequency thresholds makes GFAs ineffective in protecting system frequency in the presence of shallow frequency deviation.

- The system response with the right-biased supply curve from online GFAs is almost the same as that without any GFAs. This shows that the contribution of GFAs is negligible if the supply curve is right-biased. In addition, there is no negative impact to the system response.

- The system response with the left-biased supply curve from online GFAs is actually worse than the response without any GFAs. When the supply curve is left-biased, the power reduction from GFAs is so large that it introduces negative impact to the system response. Although it is rare to have such a supply curve, it could cause instability if it occurs. There should be a way to detect and avoid such a scenario.

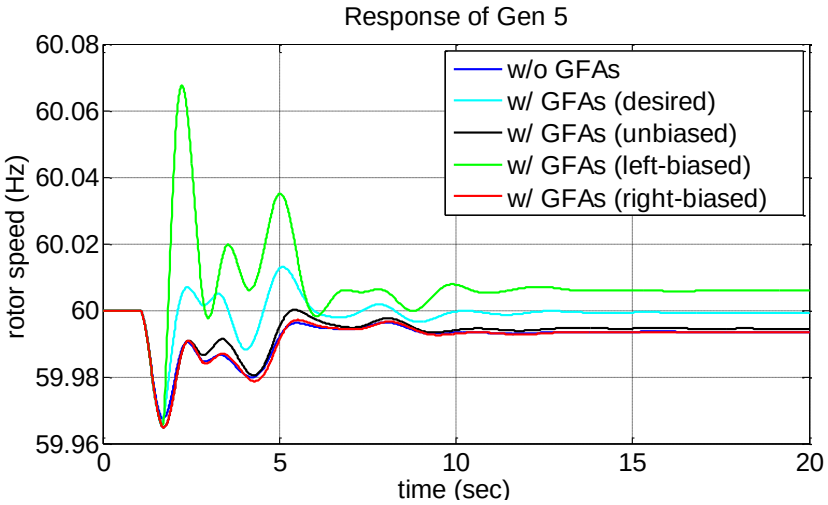

Figure 18 Rotor speed response of generator G5 in Case I

Case II: In the second case study, the same comparison is performed as in Case I while considering large disturbance. The under-frequency event in this case study is caused by the tripping of generator G12. Since the capacity of generator G12 is large, the resulting frequency deviation is beyond 59.95 Hz. Figure 19 shows the rotor speed responses of generator G5 in this case. It can be seen that when the frequency deviation is large, the system response with GFAs is greatly improved compared to the response without any GFAs. Furthermore, the system responses with different supply curves from online GFAs are quite similar to each other. The only difference is how fast the system frequency starts to recover. The system response with the left-biased supply curve has the fastest recovery speed, and the one with the right-biased supply curve has the slowest recovery speed.

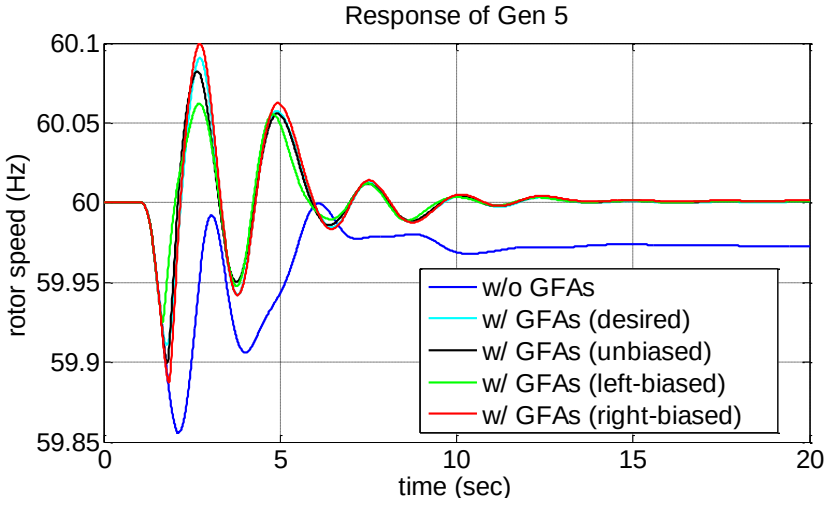

Figure 19 Rotor speed response of generator G5 in Case II

Case III: In the third case study, the system responses under different penetration levels of online GFAs are compared, where the supply curve is considered to be the unbiased. Two under-frequency events as in Case I and Case II are considered. Figure 20(a) shows the rotor speed responses of generator G5 when the system is subject to small disturbance, while Figure 20(b) shows that when the system is subject to large disturbance. The simulation results confirm further the issue associated with high penetration level of online GFAs as in [10]. The cause of this issue is because the range of curtailing frequency thresholds is fixed regardless of the penetration level of online GFAs. With higher penetration level, there will be more online GFAs to be triggered than needed, which is definitely detrimental to the system response. Therefore, it is necessary to make the range of the thresholds adaptive to the penetration level of online GFAs in the system. When the penetration level of online GFAs increases, the range of the thresholds should be enlarged and the thresholds of online GFAs should be re-sampled from this enlarged range. A potential solution to this issue will be proposed in the next section.

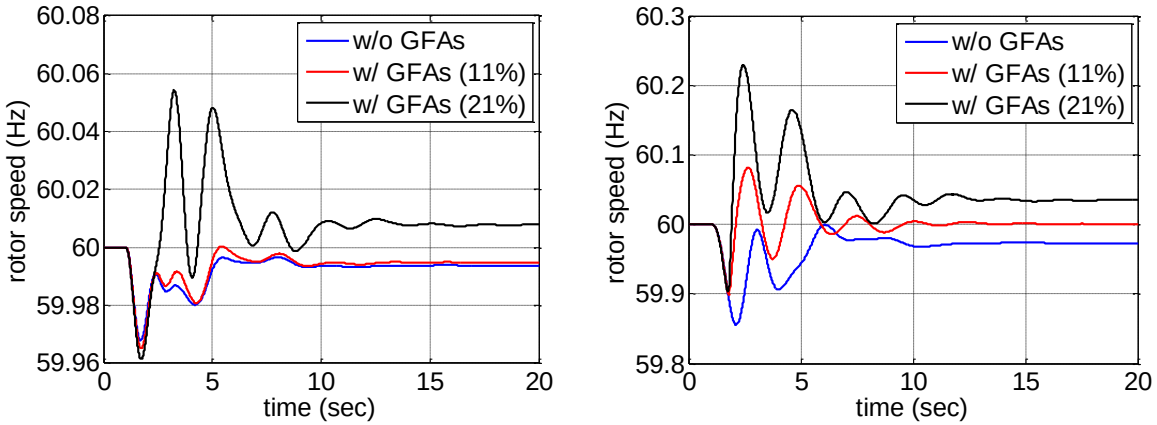

(a) Small disturbance (b) Large disturbance

Figure 20 Rotor speed response of generator G5 in Case III

4.4 A potential improvement to the GFA controller design

When under-frequency events occur, the GFA controller performs the similar function as the under-frequency relay at the substations, but with higher frequency thresholds. Thus, the objective of deploying GFAs within the system is to protect system frequency by recognizing those frequent, shallow frequency excursions. As illustrated by previous simulation studies, the power reduction of online GFAs does help improve the system response when the frequency deviates beyond the pre-specified range of curtailing frequency thresholds. However, when the frequency deviation is within that range, the current method of selecting curtailing frequency thresholds will most likely make GFAs less than ideal in protecting system frequency. Moreover, there could be negative impacts on the system response if the supply curve of online GFAs is left-biased, which could potentially render the system unstable. Although the chance of having such a scenario is very low, it is still worth the effort to prevent it from occurring.

In order to overcome the problems associated with curtailing frequency thresholds, a supervisor can be introduced at each distribution feeder to systematically monitor the GFAs under the feeder. For every time period of certain length (e.g., 15 or 30 minutes), the supervisor can collect the curtailing frequency thresholds and power ratings of those GFAs that are currently ON. Based on the collected information,

the supervisor can construct the supply curve to check if the potential power reduction of online GFAs is the desired amount. If it is indeed the case, the supervisor will alert the GFAs under its supervision, and require online GFAs to update their curtailing frequency thresholds. This mandatory update can be achieved in two different ways.

The first method is to let each online GFA randomly pick a new curtailing frequency threshold from the range again. Then the supervisor can collect the latest information to examine the new supply curve. This process will be repeated until the new supply curve is satisfactory. The second method is that the supervisor determines curtailing frequency thresholds for online GFAs as illustrated in Figure 21, where the supply curve of online GFAs is forced to be the desired one. Then each online GFA will receive the new thresholds from the supervisor and make the changes locally.

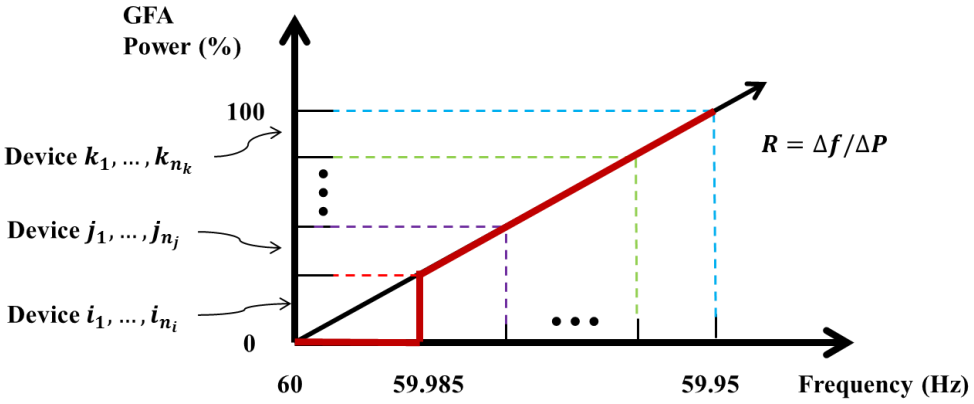

Figure 21 Curtailing frequency threshold determination by the supervisor

In order to overcome the overreacting issue resulting from the high penetration level of online GFAs, it is necessary to make the range of the thresholds adaptive to the penetration level. One way to realize the adaptive range for curtailing frequency thresholds is through the supervisor just introduced. After collecting power ratings of online GFAs at the beginning of each period, supervisors located at different feeders can utilize information discovery algorithms to determine the total power of online GFAs in the system. For example, the supervisors can run consensus algorithms by exchanging the current power of online GFAs under their supervision with neighboring supervisors. Once the total power of online GFAs is known, each supervisor can determine a new range accordingly and then broadcast it to the supervised GFAs, which will randomly pick a curtailing frequency threshold from this new range. The selection of appropriate range for a given penetration level of online GFAs will be investigated in the future.

5.0 Conclusions

An improved hierarchical frequency based load control strategy was proposed that uses only local frequency measurements and is adaptive to changing system operating conditions. A rigorous theoretical analysis is performed to prove the closed-loop system stability under demand-side frequency control. In particular, it was shown that if the post fault equilibrium of the power system without demand-side frequency control is asymptotically stable, then the post-fault equilibrium of the power system coupled with demand-side frequency control is also asymptotically stable if the gains are selected to be nonnegative. The proposed control strategy was implemented and tested on the WECC model in PowerWorld. The results indicated that:

- Proposed control leads to an improved frequency recovery in terms of steady state error and maximum frequency deviation as compared to the case without load control
- Intertie power flow response depends on relative location of disturbance and percentage of responsive load/generation
- Load control could be used as additional resource in areas with lack of generation (e.g., southern WECC in summer)
- Dynamics of different types of end-use loads (i.e., HVAC vs. water heaters) affect control performance
- Control gain can be adapted based on changing operating conditions and desired penetration levels

The impacts of frequency responsive GFAs on bulk power system are analyzed further by examining the curtailing frequency threshold, which is another important design parameter of the GFA controller. It was shown that when the actual distribution of the pre-determined thresholds is biased, it could potentially impact the system response negatively. Based on the performed analysis, one possible solution was to introduce a supervisor at each distribution feeder to systematically monitor the state of the system. Whenever necessary, the supervisor can modify the thresholds of all the supervised GFAs in such a way that their autonomous responses will be coordinated to avoid any potential negative effects. It was concluded that it is necessary to make the range of the thresholds adaptive to the penetration level of online GFAs in the system.

6.0 Future Work

In FY15, some of the next steps include:

- Analyzing interactions of proposed control strategy integrated with primary and secondary generator frequency controls and under-frequency load shedding schemes
- Studying voltage "side effects" i.e., unintended consequences related to inherent modulation of reactive component of load while load is under primary frequency control
- Including an improved representation of the distribution network and detailed models of the end-use loads (e.g.; WECC composite load model or combine with feeder models in GridLAB-D)
- Implementing proposed hierarchical control strategy in integrated transmission & distribution environment (e.g., PowerWorld+ GridLAB-D)
- Continuing to investigate the new GFA controller design and implement it in PowerWorld on the WECC system model, followed by performing extensive simulation studies to confirm FY14 findings regarding system response characterization
- Developing a roadmap that outlines a strategy engaging various stakeholders (e.g., industry, utilities, WECC)

References

[1] M Donnelly, S Mattix, D Trudnowski and JE Dagle, "Autonomous Demand Response for Primary Frequency Regulation," PNNL-21152, 2012, Pacific Northwest National Laboratory, Richland, WA.

[2] K Kalsi, W Zhang, J Lian, LD Marinovici, C Moya, and JE Dagle, "Distributed Smart Grid Asset Control Strategies for Providing Ancillary Services," PNNL-22875, 2013, Pacific Northwest National Laboratory, Richland, WA.

[3] Molina-Garcia, F. Bouffard and D. S. Kirschen, "Decentralized demand-side contribution to primary frequency control," *IEEE Trans. On Power Systems*, vol. 26, no. 1, pp. 411-419, 2001.

[4] C. Zhao, U. Topcu, and S. Low, "Frequency-based load control in power systems," in *American Control Conference (ACC), 2012*, 2012, pp. 4423–4430.

[5] C. Zhao, U. Topcu, and S. Low, "Swing dynamics as primal-dual algorithm for optimal load control," in *Smart Grid Communications (SmartGridComm), 2012 IEEE Third International Conference on*, 2012, pp. 570-575.

[6] C. Zhao, U. Topcu, and S. Low, "Fast load control with stochastic frequency measurement*," IEEE Power and Energy Society General Meeting*, 2012.

[7] R. Diao, M. Elizondo, E. Mayhorn and Y. Zhang, "Electric water heater modeling and control strategies for demand response", *Power and Energy Society General Meeting, 2012 IEEE*, 2012, pp. 1–8.

[8] D. J. Hammerstrom, J. Brous, D. P. Chassin, G. R. Horst, R. Kajfasz, P. Michie, T. V. Oliver, T. A. Carlon, C. Eustis, O. M. Jarvegren, W. Marek, R. L. Munson, and R. G. Pratt, "Pacific Northwest GridWise Testbed Demonstration Projects; Part II. Grid Friendly Appliance Project," PNNL-17079, 2007, Pacific Northwest National Laboratory, Richland, WA.

[9] D. J. Hammerstrom, R. Ambrosio, T. A. Carlon, J. G. DeSteese, G. R. Horst, R. Kajfasz, L. L. Kiesling, P. Michie, R. G. Pratt, M. Yao, J. Brous, D. P. Chassin, R. T. Guttromson, O. M. Jarvegren, S. Katipamula, N. T. Le, T. V. Oliver, and S. E. Thompson, "Pacific Northwest GridWise Testbed Demonstration Projects; Part I. Olympic Peninsula Project," PNNL-17167, 2007, Pacific Northwest National Laboratory, Richland, WA.

[10] K. Kalsi, J. Lian, C. Moya, W. Zhang, L. D. Marinovici and J. E. Dagle, "Distributed Smart Grid Asset Control Strategies for Providing Ancillary Services," PNNL-22875, 2013, Pacific Northwest National Laboratory, Richland, WA.

[11] N. Lu, D. J. Hammerstrom, and S. Patrick, "Grid Friendly™ Device Model Development and Simulation," PNNL-18998, 2009, Pacific Northwest National Laboratory, Richland, WA.

[12] A. R. Bergen, Power systems analysis. Prentice-Hall series in electrical and computer engineering. Prentice Hall, Englewood Cliffs (N.J.), 1986.

[13] A.R. Bergen and D.J. Hill. A structure preserving model for power system stability analysis. *Power Apparatus and Systems, IEEE Transactions on*, PAS-100(1):25–35, 1981.

[14] D.J. Hill and A.R. Bergen. Stability analysis of multimachine power networks with linear frequency dependent loads. *Circuits and Systems, IEEE Transactions on*, 29(12):840–848, 1982.

[15] C. Moya, W. Zhang, J. Lian, and K. Kalsi, "A hierarchical framework for demand-side frequency control," *American Control Conference (ACC), 2014* , vol., no., pp.52,57, 4-6 June 2014.

[16] F. Dörfler and F. Bullo. "Synchronization in Complex Oscillator Networks: A survey". *Automatica*, 50(6), June 2014

[17] N Lu, DJ Hammerstrom, "Design Considerations for Frequency Responsive Grid Friendly™ Appliances", *2005/2006 IEEE/PES Transmission and Distribution Conference and Exhibition, 2006*, Dallas, TX, pp. 647-652.
[18] G. Rogers, Power System Oscillations. 101 Philip drive, Assinippi Park, Norwelll, MA 02061: Kluwer Academic Publishers, 2000.
[19] J. Chow and G. Rogers, Power System Toolbox, 3rd ed., 1991-2008. [Online]. Available: http://www.eps.ee.kth.se/personal/vanfretti/pst/Power System Toolbox Webpage/PST.html
[20] PowerWorld Simulator software, http://www.powerworld.com
[21] Siemens PTI PSS/E software, https://w3.siemens.com/smartgrid/global/en/products-systems-solutions/software-solutions/planning-data-management-software/planning-simulation/Pages/PSS-E.aspx
[22] GE PSLF software, http://www.geenergyconsulting.com/practice-area/software-products/pslf
[23] FS Chassin, ET Mayhorn, MA Elizondo, S Lu, "Load modeling and calibration techniques for power system studies," North American Power Symposium (NAPS), 2011
[24] "Western Electricity Coordinating Council Off-Nominal Frequency Load Shedding Plan", May 2011

Distribution

1 Phil Overholt
Department of Energy, OE
1000 Independence Ave., SW
Routing OE-10
Washington, DC 20585

1 Wei Zhang
404 Dreese Labs,
2015 Neil Ave.,
Columbus, OH, 43210
(PDF copy)

7 **Local Distribution**
Pacific Northwest National Laboratory

Karanjit Kalsi	(PDF)
Jianming Lian	(PDF)
Laurentiu Marinovici	(PDF)
Marcelo Elizondo	(PDF)
Jeff Dagle	(PDF)
Robert Pratt	(PDF)
Jason Fuller	(PDF)

Pacific Northwest
NATIONAL LABORATORY

Proudly Operated by **Battelle** *Since 1965*

U.S. DEPARTMENT OF
ENERGY

902 Battelle Boulevard
P.O. Box 999
Richland, WA 99352
1-888-375-PNNL (7665)

www.pnnl.gov